NAVAL POSTGRADUATE SCHOOL
Monterey, California

94-09401

THESIS

DTIC
ELECTE
MAR 2 8 1994
S B D

THERMOSPHERIC

MODELING ACCURACIES

USING

F10.7 & Ap

by

John J. Adler

December, 1993

Thesis Advisor: I. M. Ross

Thesis Co-Advisor: R. C. Olsen

Approved for public release; distribution is unlimited.

94 3 25 083

DTIC QUALITY INSPECTED 3

REPORT DOCUMENTATION PAGE		Form Approved OMB No. 0704

Public reporting burden for this collection of information is estimated to average 1 hour per response, including the time for reviewing instruction, searching existing data sources, gathering and maintaining the data needed, and completing and reviewing the collection of information. Send comments regarding this burden estimate or any other aspect of this collection of information, including suggestions for reducing this burden, to Washington Headquarters Services, Directorate for Information Operations and Reports, 1215 Jefferson Davis Highway, Suite 1204, Arlington, VA 22202-4302, and to the Office of Management and Budget, Paperwork Reduction Project (0704-0188) Washington DC 20503.

1. AGENCY USE ONLY *(Leave blank)*	2. REPORT DATE 15 December 1993	3. REPORT TYPE AND DATES COVERED Master's Thesis
4. TITLE AND SUBTITLE Thermospheric Modeling Accuracies Using Forecasted F10.7 and Ap		5. FUNDING NUMBERS
6. AUTHOR(S) Adler, John J.		
7. PERFORMING ORGANIZATION NAME(S) AND ADDRESS(ES) Naval Postgraduate School Monterey CA 93943-5000		8. PERFORMING ORGANIZATION REPORT NUMBER
9. SPONSORING/MONITORING AGENCY NAME(S) AND ADDRESS(ES)		10. SPONSORING/MONITORING AGENCY REPORT NUMBER

11. SUPPLEMENTARY NOTES The views expressed in this thesis are those of the author and do not reflect the official policy or position of the Department of Defense or the U.S. Government.

12a. DISTRIBUTION/AVAILABILITY STATEMENT Approved for public release; distribution is unlimited.	12b. DISTRIBUTION CODE A

13. ABSTRACT *(maximum 200 words)*
This thesis analyzes the accuracy of the 45 day forecasted F10.7 and Ap values given by the Air Force Space Forecast Center. These forecasts are generated daily to aid many agencies in their fields of endeavor. The U.S. Space Command uses the values in orbit prediction routines by way of atmospheric density models. This thesis shows that the F10.7 forecasts are accurate from one to seven days out, then deteriorate for the latter 38 days. Conversely, Ap forecasts are less accurate from one to five days out, then improve beyond the sixth day. The effects of forecasting errors upon satellite lifetimes are then shown using the Lifetime 4.1 orbital propagation model with a Jacchia '71 atmosphere. Propagating a typical satellite for 45 days over various configurations of altitudes and eccentricities showed that only a narrow altitude band from $250 km$ to $325 km$ is affected. Regions above or below this band are not significantly affected with errors in F10.7 or Ap.

14. SUBJECT TERMS Thermosphere; F10.7; Ap; Satellite Re-entry; Orbit Perturbations; Atmospheric Density			15. NUMBER OF PAGES 72
			16. PRICE CODE
17. SECURITY CLASSIFICATION OF REPORT Unclassified	18. SECURITY CLASSIFICATION OF THIS PAGE Unclassified	19. SECURITY CLASSIFICATION OF ABSTRACT Unclassified	20. LIMITATION OF ABSTRACT UL

THERMOSPHERIC
MODELING ACCURACIES
USING
F10.7 & Ap

by

John J. Adler

Lieutenant, United States Navy

B.S., University of California, Santa Barbara, 1987

B.A., University of California, Santa Barbara, 1987

Submitted in partial fulfillment

of the requirements for the degree of

MASTER OF SCIENCE IN PHYSICS

from the

NAVAL POSTGRADUATE SCHOOL

December 1993

Author: _____
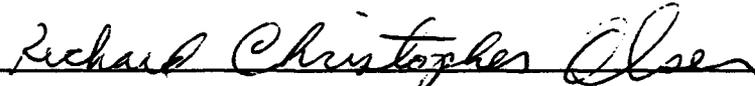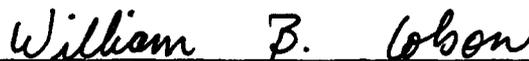
John J. Adler

Approved by: _____

I. M. Ross, Thesis Advisor

_____

R. C. Olsen, Co-Advisor

_____

W. B. Colson, Chairman

Department of Physics

ABSTRACT

This thesis analyzes the accuracy of the 45 day forecasted F10.7 and Ap values given by the Air Force Space Forecast Center. These forecasts are generated daily to aid many agencies in their fields of endeavor. The U.S. Space Command uses the values in orbit prediction routines by way of atmospheric density models. This thesis shows that the F10.7 forecasts are accurate from one to seven days out, then deteriorate for the latter 38 days. Conversely, Ap forecasts are less accurate from one to five days out, then improve beyond the sixth day. The effects of forecasting errors upon satellite lifetimes are then shown using the Lifetime 4.1 orbital propagation model with a Jacchia '71 atmosphere. Propagating a typical satellite for 45 days over various configurations of altitudes and eccentricities showed that only a narrow altitude band from $250km$ to $325km$ is affected. Regions above or below this band are not significantly affected with errors in F10.7 or Ap.

TABLE OF CONTENTS

ACKNOWLEDGMENTS

I especially would like to thank Robin for her considerable efforts in helping me get this completed. I would also like to thank Kevin and Donna for their support in many ways during this study. And finally I would like to thank Bev and Bud for their help throughout my tour at the Naval Postgraduate School.

I. INTRODUCTION

A. BACKGROUND

The Air Force Space Command Headquarters at Peterson AFB is tasked with cataloguing all artificial earth satellites, be they U.S. or foreign in origin. One sub-task of this momentous job is predicting the satellite positions in space and time (ephemeris), including their possible re-entry into the earth's atmosphere. Determination of the most probable impact point is also sometimes necessary. Increasing the accuracy of satellite ephemeris, both in actual measurements and in predictive capabilities, is a constant goal for the Space Command.

All satellites' motions are influenced by the same key parameters: gravity, ballistic coefficient, atmospheric density, actual position, and actual velocity. Algorithms have been written over the years to determine each of these parameters as accurately as possible, some have been modeled with great success.

The earth's gravitational potential has been split and re-split from a simple spherical body into a tesseral harmonic model. Tesseral harmonics allows for gravitational compensation due to local terrain anomalies such as mountains and oceans, as well as general global deviations such as the oblong elliptical shape of the longitudal direction.

The ballistic coefficient $B = \dfrac{m}{C_d A}$ takes into account both a changing coefficient of drag, C_d, and changing vehicle profile area, A, which is the surface area of a satellite with the normal vector parallel to the velocity vector. The coefficient of drag can vary from 3.0 in a free flow regime to less then 1.0 in a continuum flow. Changes in both factors occur in normal spaceflight, therefore B is typically a variable parameter; further research is currently attempting to remove ambiguities in this area. However, there is a general

1

tendency to use this variable as residue factor that absorbs deficiencies in the other variables, such as the atmospheric density and geopotential. Consequently, it is quite a struggle to decouple this factor, or conversely, it is troublesome to perfect another variable when B is changing with respect to it.

Atmospheric density also has been split into increasingly finer gradations in an attempt to create an accurate working model. These divisions include description of density changes as altitude increases, the addition of atmospheric heating inputs, and the modeling of global circulation patterns. Atmospheric density, ρ, enters into the orbital equations through a perturbation acceleration [Ref. 5: p. 142]:

$$a_D = -\frac{1}{2}\rho\left(\frac{C_d A}{m}\right)v^2 \qquad \text{(Eq 1)}$$

Two of the most frequently used parameters for modeling in the thermosphere are the F10.7 solar flux index and the Ap geomagnetic index. F10.7 is a radio frequency observation of the sun that indirectly indicates the amount of solar activity, and consequently the degree of atmospheric heating. This parameter aids in indicating the amount of drag a satellite experiences due to thermospheric density. F10.7 is a direct measurement made of solar flux by radio telescopes in Canada at $10.7cm$ wavelength ($2.8GHz$). The units are $\cdot 10^{-22}\frac{W}{m^2 Hz}$. The values typically range between 70 and 220 for a quiescent or active sun, respectively.

The Ap index indicates the magnitude of magnetic activity on the earth, which is the second largest input to the thermospheric heating equation. This parameter also influences the drag encountered by a satellite. Ap is an indirect measurement of current flowing in the ionosphere made by averaging the measurements of 12 magnetic observatories located worldwide. The units are in nanoTeslas (nT).

2

B. PROBLEM STATEMENT

Air Force Space Forecast Center, Falcon AFB, generates predicted values for F10.7 and Ap daily. These predicted values are for the next 45 days. Each day in the future is given a predicted F10.7 and Ap value. These values are used by many agencies for many reasons: prediction of maximum usable frequencies, prediction of solar flares, etc. The U.S. Space Command uses these values in their orbit propagation routines to predict satellite ephemeris. If the forecasts are 100% accurate, then any deviation of the predicted satellite ephemeris from the actual satellite ephemeris is a result of modeling errors. Many studies have been made to determine modeling errors by comparing actual ephemeris to predicted ephemeris. This thesis instead looks to determine the predicted F10.7 and Ap errors throughout the 45 day forecasted period, and then apply them to a currently used atmospheric model (Jacchia '71), and determine how these errors affect the propagation routines.

C. OBJECTIVES

This thesis looks to analyze and determine the errors in the 45 day forecasted F10.7 and Ap. Specifically, to determine:

- the average error for each predicted day-out, from 1 day-out to 45 days-out

- the standard deviation for each predicted day-out, from 1 day-out to 45 days-out

- the number of predictions landing in six bins labeled excellent, good, average, poor, unsatisfactory, and terrible

Additionally this thesis looks to determine the impact of forecasted errors in F10.7 and Ap upon a satellite propagation model, Lifetime 4.1, determining:

- difference in total number of revolutions made over a 45 day period

- difference in the perigee altitude over a 45 day period

3

II. OVERVIEW

This chapter is an overview of the terminology which will be used and gives a brief orientation of the solar and terrestrial configurations. The first section defines the structure of the solar and terrestrial bodies and their atmospheres. The following section expands upon solar and terrestrial environments and describes the electromagnetic interaction processes involved. The last section describes the indexes, F10.7 and Ap, representing these activities.

A. TERMINOLOGY AND ORIENTATION

1. Solar Anatomy

The sun is typically characterized as a $6000K$ homogenous black body. However, its internal structure is quite complex, and its temperature varies considerably throughout its interior. Six general regions, listed radially from the central core to the outer circumference, describe the major sections of the sun: the core, radiative interior zone, convection zone, photosphere, chromosphere, and corona (Figure 1) . What one sees when looking at the sun visually is the photosphere, a thin layer approximately $500km$ deep that defines the edge of the sun as we normally think of it. Its temperature is approximately $6000K$ and has its peak radiation frequency in the visible band. Above this region is the chromosphere, about $2500km$ thick with a temperature of $2 \cdot 10^4 K$. The final layer of the sun's atmosphere is the corona, which extends out several solar radii and has a temperature of $2 \cdot 10^6 K$ The chromosphere, and especially the corona, have extremely low densities and are transparent to the naked eye.
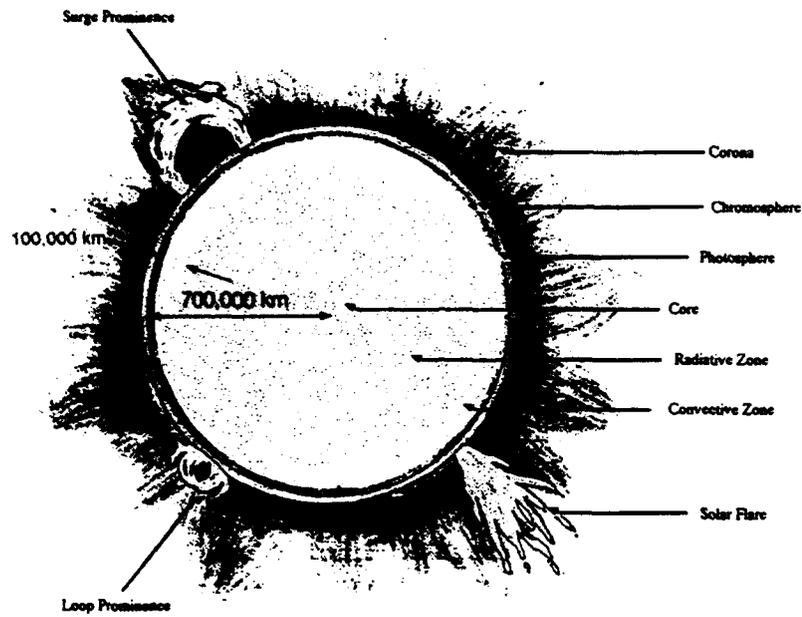
Figure 1: The Sun [Ref. 14: p. 442]

2. Terrestrial Anatomy

The earth's atmosphere is classically divided into four regions based upon temperature and pressure gradients: the troposphere, stratosphere, mesosphere, and thermosphere. The upper limits (boundaries) for each region are called the tropopause, stratopause, mesopause, and thermopause, respectively [Ref. 10: p. 109]. Figure 2 depicts these regions. Beyond the thermopause is the region referred to as the exosphere, of extreme low density and low temperature, and is the transition into space.

The earth's atmosphere is alternatively classified into two regions, known as the homosphere and the heterosphere. The transition region between the two is called the turbopause; the altitude differentiating these two regions does not correspond to any of the four previously mentioned divisions. Again, the region beyond the heterosphere is known as the exosphere, from $500km$ to $1000km$. Figure 3 shows in detail the various regions.
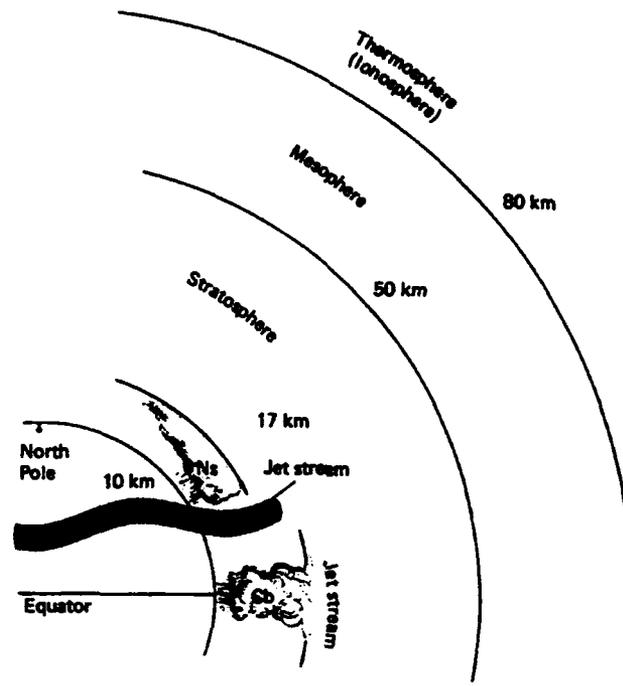
5

Figure 2: The Earth's Atmosphere [Ref. 15: p. 109]

Temperature measurements in these regions refers to the total energy of the individual particles. It is not the "temperature" to which we generally associate with a thermometer. In these cases, although the temperature is high, the heat content is low. A thermometer measures the average temperature of the many millions of particles with which it comes into contact. The density of particles on earth is quite high, typically $1.2\frac{kg}{m^3}$. As each particle hits the thermometer it raises the temperature an imperceptible amount; the combination of millions of particles will then give us the "room temperature" as we know it. In the upper terrestrial and solar atmospheres the particle densities are quite low, about $4.76 \cdot 10^{-13}\frac{kg}{m^3}$ and $1 \cdot 10^{-9}\frac{kg}{m^3}$ respectively. If a thermometer was placed into these regions it would rarely encounter a particle, and when struck the temperature would only imperceptibly raise. Consequently, space is sensibly quite cold to us, though we can refer to some regions as reaching temperatures of $1500K$.
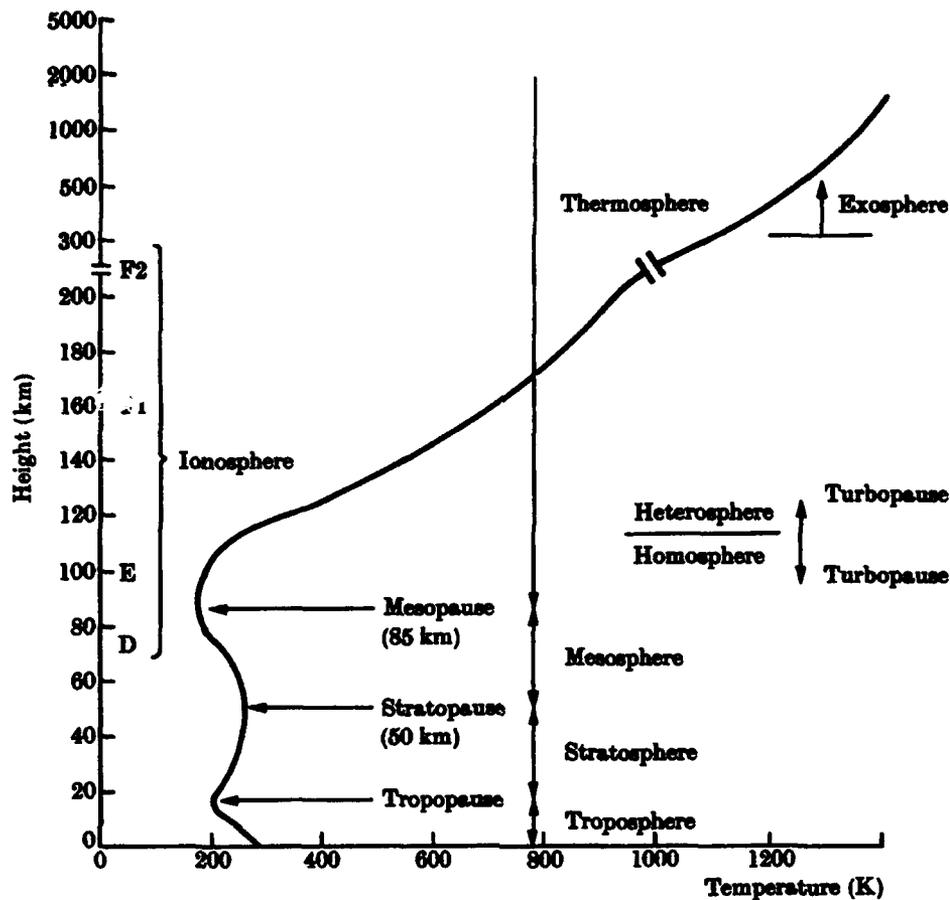
Figure 3: Atmospheric Categories [Ref. 10: p. 111]

a. Troposphere

The troposphere is the atmosphere as we generally think of it, characterized by intense convection and cloud formations. It extends from the surface of the earth up to $10km$ over the poles, and up to $16km$ over the equatorial regions. Here normal lapse rates occur, temperature and density both decrease with altitude.

b. Stratosphere

The stratosphere is located above the tropopause up to $50km$ in altitude. This region contains atmospheric ozone, which is a strong absorber in the extreme ultraviolet (EUV), and one reason why direct measurements of EUV can not be made from the ground. Due to the absorption, the stratosphere contains a positive temperature grad.. `t, but the pressure continues to decrease with altitude.

c. Mesosphere

The mesosphere is located above the stratopause up to $80km$ in altitude. It has a negative pressure and temperature gradient, generating at the mesopause the coldest temperature located in the atmosphere ($180K$).
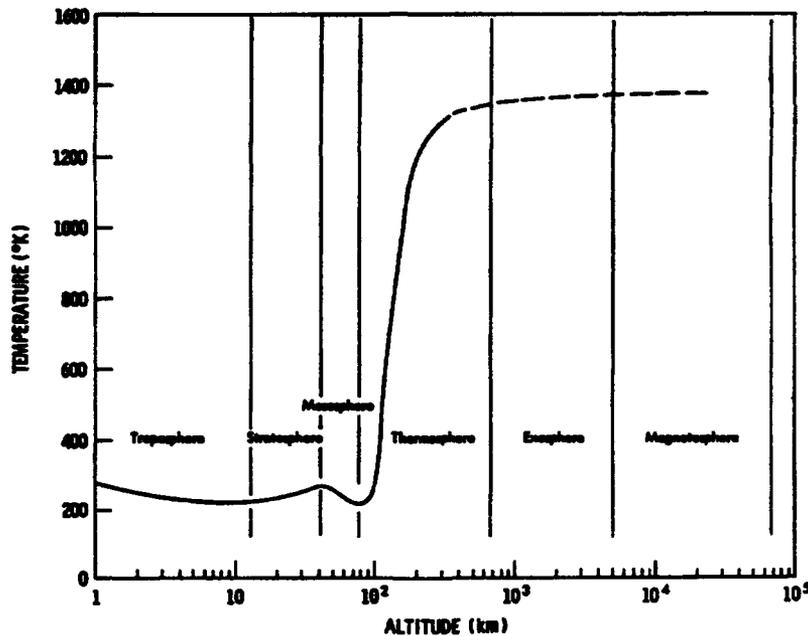

Figure 4: Atmospheric Temperature Changes [Ref. 11: p. 679]

d. Thermosphere

The thermosphere extends from the mesopause up to $500km$ in altitude. Temperature here increases with altitude, while pressure continues to decrease. Temperatures can be as high as $1500K$ at $300km$. It is in this region that satellite positioning is most difficult to predict. Below the thermosphere, the density is so large that satellites typically re-enter within 2 revolutions. Above the thermosphere density is so low that it is a second order effect behind solar radiation pressure, and is therefore difficult to model accurately. Additionally, in the thermosphere, density fluctuates quite drastically with temperature changes. Figure 4 shows the overall temperature profile (note increasing altitude is on the logarithmic X axis), Figure 5 shows the density and pressure profiles (note increasing altitude is on the Y axis).
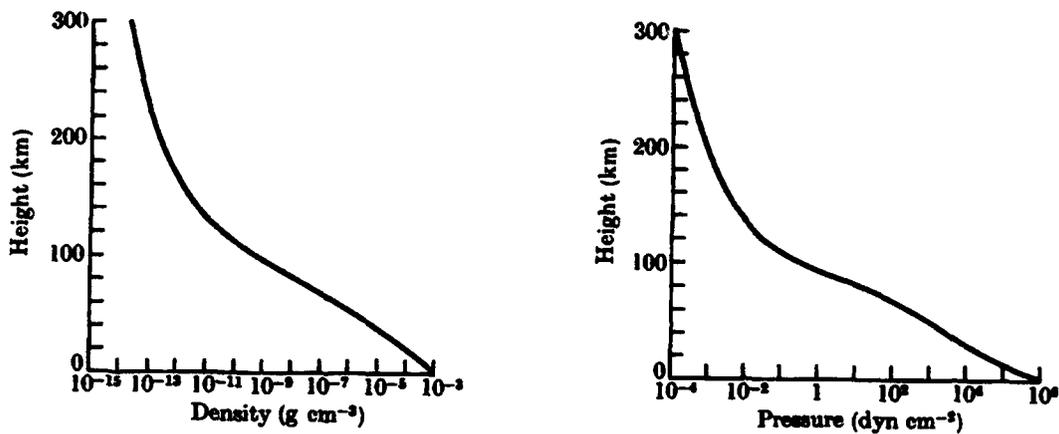
Figure 5: Atmospheric Density & Pressure Changes [Ref. 10: p. 110]

e. Homosphere

The homosphere exists from ground to $100km$. The name is derived from the uniformity of concentration of the atmospheric constituents: 78% N, 21% O_2, 1% Ar plus trace amounts of other gases. This uniformity exists because thermal gradients throughout

9

the region cause turbulent mixing, preventing layering of the gases. Above $90km$ two factors destroy homogeneity: oxygen disassociation and the diffusion process. Disassociation occurs when the O_2 molecule is energized and splits into atomic oxygen, $2O$. It happens at the altitude where the density is low enough to allow $0.1\mu m$ to $0.2\mu m$ radiation pass [Ref. 2: p. 157]. At low densities, recombination due to collisions is infrequent, and the survival rate of atomic oxygen rises as altitude increases. The O/O_2 ratio is 0.02 at $90km$, 0.08 at $95km$, and 0.22 at $100km$. At this altitude the density is so low that turbulent mixing ceases and the transition to the heterosphere begins. This boundary is known as the turbopause, and has an extremely stable lapse rate.

f. Heterosphere

The heterosphere exists from $100km$ to $500km$ and is where diffusion of the present gases takes place. Molecularly heavy particles stay at a lower altitude while lighter ones continue to escape upwards. The actual distribution functions, called scale heights, are found by equating the pressure gradient of the atmosphere with the gravitational force, as shown from the perfect Gas Law,

$$P = \left(\frac{\rho}{m}\right)kT \qquad\qquad \text{(Eq 2)}$$

where P = gas pressure, k = Boltzman constant, m = molecular mass, T = temperature, and ρ = density. For a small cross sectional area thickness dh

$$dP = -\rho g dh \qquad\qquad \text{(Eq 3)}$$

therefore

$$\frac{dP}{P} = \frac{d\rho}{\rho} + \frac{dT}{T} \qquad\qquad \text{(Eq 4)}$$

10

$$-dh = \frac{kT}{mg}\left(\frac{d\rho}{\rho} + \frac{dT}{T}\right) \qquad \text{(Eq 5)}$$

Assuming isothermal variation, and letting the scale height, H, be defined as: $H = \dfrac{kT}{mg}$, we get a simple differential equation

$$\frac{d\rho}{\rho} = -\frac{1}{H}dh \qquad \text{(Eq 6)}$$

with solution

$$\rho = e^{-\frac{1}{H}h}e^{C} \qquad \text{(Eq 7)}$$

letting $e^{c} = \rho_0$, we get

$$\rho = \rho_0 e^{-\frac{1}{H}h} \qquad \text{(Eq 8)}$$

as the final solution. Each molecule type will have a different scale height depending upon its mass, other things held constant. From Eq. 8 we can conclude that the density of each constituent will fall off at different levels, and hence the layering or diffusive effect. Argon, mass 40, decreases 10 times faster than helium, mass 4. Molecular oxygen, mass 32, will decrease twice as fast as atomic oxygen, mass 16. However, in oxygen's case, diffusion coupled with disassociation takes place. O quickly becomes more abundant than O_2 at only 110 km. (The density of the constituents here is so low, collisions are at a minimum and recombination of O plays a very minor part). The diffusion process continues, a layering takes place amongst Ar, O_2, N_2, O, He, and H, in that order, as altitude increases. Figure 6 shows the density of each constituent.
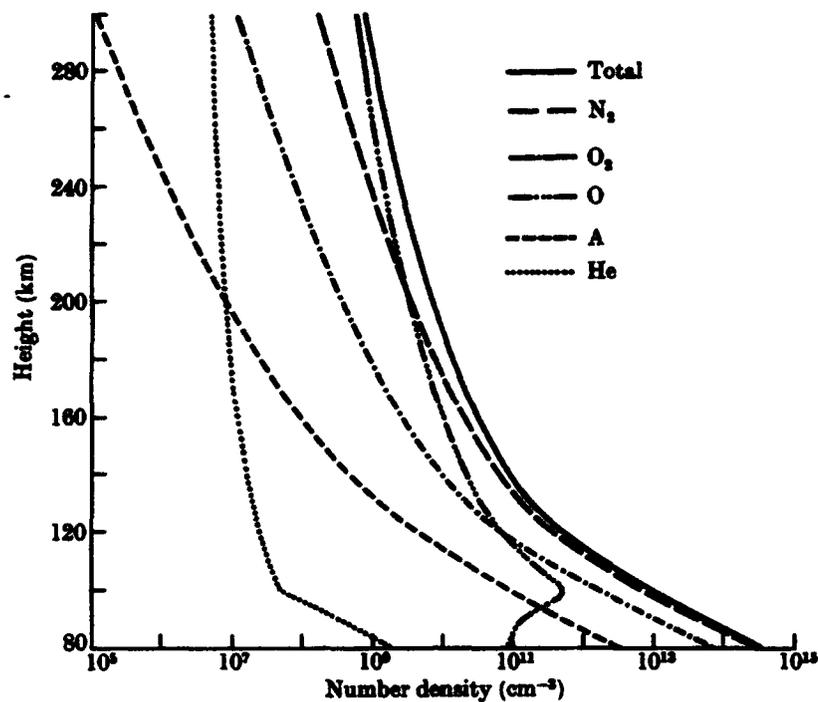
Figure 6: [Ref. 10: p. 110]

B. SOLAR PHYSICS

Since the sun is not characterized with a homogenous makeup, each different region has a different thermal energy, or temperature. Although the bulk of solar radiation comes from the photosphere, other regions contribute in significant ways. Looking at the solar radiation curve over all frequencies, we see it is not a $6000K$ blackbody. The chromosphere and corona, with temperatures of approximately $2 \cdot 10^6 K$ contribute to the blackbody radiation curve EUV range ($\lambda = 10 - 100nm$). As seen in Figure 7 this is a highly variable output that can differ by over an order of magnitude depending upon the current state of the solar cycle.
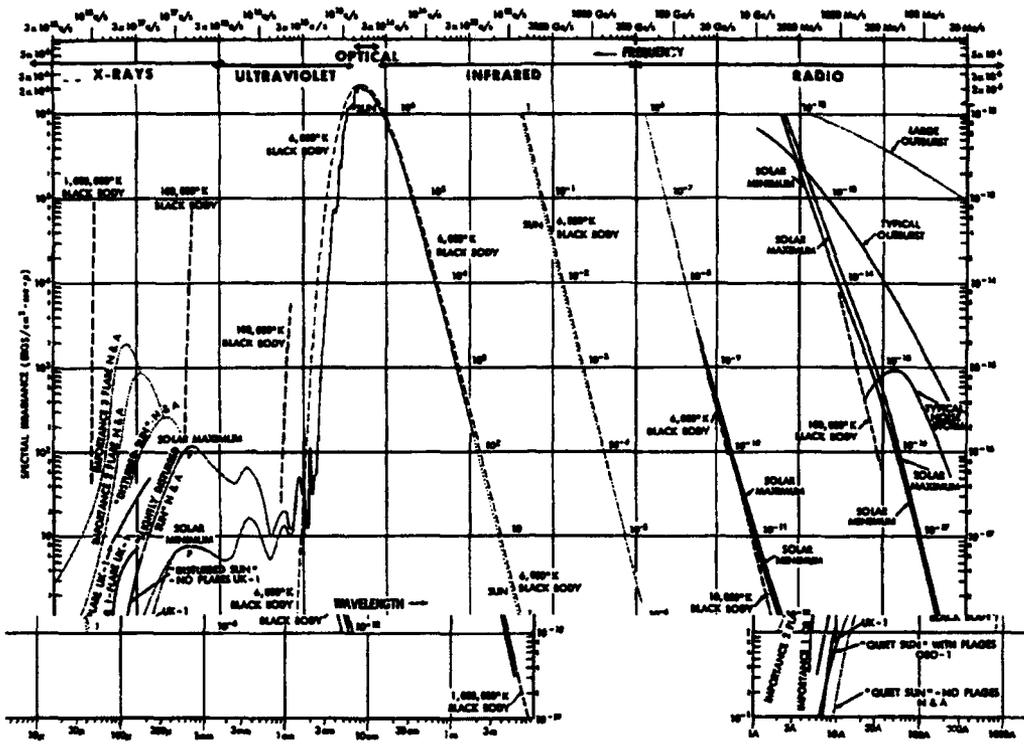
Figure 7: Solar Spectral Irradiance [Ref. 11: p. 592]

A rough guide to the distribution of the solar spectral output by percentage is:

- $1 \cdot 10^{-8}\%$ RF

- 52% IR

- 41% Visible

- 7% Near IR

- 0.1% Far UV and X-Ray

Total power of the sun over all these wavelengths is $3.82 \cdot 10^{26} W$. The power received at the earth's position is found by dividing the total power by the surface area of a shell at 1AU (which would intercept all the sun's power).

$$\text{Solar input at earth} = \frac{3.82 \cdot 10^{26} W}{4\pi (149 \cdot 10^{9} m)^2} \qquad \text{(Eq 9)}$$

13

$$\text{Incident Power} = 1358\frac{W}{m^2}$$

This is called the solar constant and does not vary by more than one or two parts in 1000. The near-invariability of radiation in the visible and infrared, which make up the majority of the solar output, is contrasted by the considerably variable EUV intensity[Ref. 2: p. 155]. The variable EUV output, even though at a maximum of two or three percent of the total solar output, has a quite profound effect upon the terrestrial atmosphere.

C. TERRESTRIAL PHYSICS

The earth's atmosphere is highly variable throughout the four atmospheric regions; this study is particularly interested in thermospheric variations. Little was known about the thermosphere until the rocket age. In fact, four of the five types of variation now known in the thermosphere where discovered through analysis of satellite drag: solar activity, daily variation, geomagnetic effect, and semi-annual effect. The fifth effect, seasonal latitudinal changes in composition, was discovered through optical methods and mass spectrometry in addition to drag analysis. [Ref. 3: p. 231] Following each section are the equations developed by Jacchia for the '71 thermospheric model and implemented by Lifetime 4.1 [Ref. 18].

1. Solar Activity

The solar output incident upon the earth is approximately 1358 $\frac{W}{m^2}$, and is fairly constant. Only a small fraction of this incident solar flux is actually absorbed in the thermosphere. This is due to the extreme low density of the terrestrial gases and the lower output by the sun in the EUV spectrum relative to the visual wavelengths.

The earth further increases the variability of incident EUV due to its rotation. At local noon the EUV contribution will be at its maximum, at local midnight it will be a

14

minimum. These wavelengths heat the thermosphere to temperatures ranging from $600K$ during the evening at low solar activity, to $2500K$ at maximum solar and geomagnetic activity in the auraol regions [Ref. 2: pp. 158-159]. On the average 50% of absorbed solar energy goes to local heating of the main constituent gases N_2, O_2, and O [Ref. 8: p. 543]. Only $1 \cdot 10^{-6}$ of the solar energy supplied to the earth is absorbed in the thermosphere [Ref. 9: p. 43].

Solar output is not consistent over solar cycles either. Although the maximum values of F10.7 are fairly consistent, the maximum values can vary by 20% to 25% between the 11 year solar cycles. This will drastically affect the annual flux averages used in satellite mission planning. Currently we are approaching a solar minimum in 1996; the last solar maximum was in 1990, the next solar maximum will be in 2001 [Ref. 5: p. 203]. Figure 8 shows the F10.7 values since the beginning of the observations; exospheric temperatures are indicated on the right Y axis.
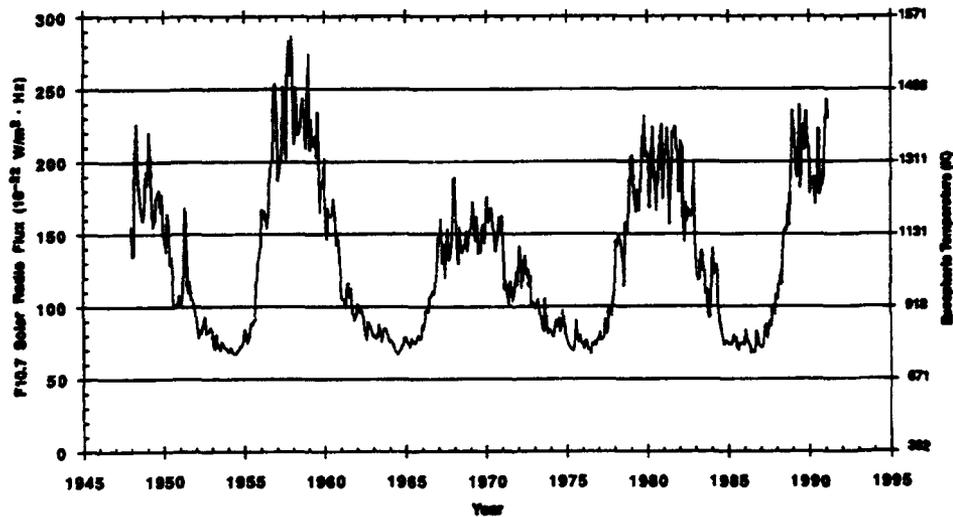

Figure 8: Composite F10.7 Flux [Ref. 5: p. 209]

15

This effect is modeled using the daily F10.7 flux value $F_{10.7}$, and the 81 day mean flux value $\bar{F}_{10.7}$. This base temperature is defined as the nighttime minimum global exospheric temperature (for Kp = 0):

$$T_c = 379 + 3.24 \cdot \bar{F}_{10.7} + 1.3 \, (F_{10.7} - \bar{F}_{10.7}) \qquad \text{(Eq 10)}$$

2. Daily Variation

The maximum density occurs near the latitude of the satellite subsolar point at the longitude that corresponds to a local time of 1420 [Ref. 4: p. 294]. This appears to be independent of altitude, but that is deceptive. Each constituent gas has a maximum density which occurs at different times of the day, and is altitude dependent. For instance, He density peaks at 0800 for an altitude of $250km$, but the peak occurs at 1400 for an altitude of $1000km$. However, when all the constituents are added up, their sum for maximum density is fairly constant at 1420 local at all heights [Ref. 4: p. 294]. The minimum density occurs at 0220 local time. At low altitudes a satellite will not experience much changes in density due to this effect, but by $600km$ a factor of 8 difference is seen between the night and daytime densities [Ref. 11: p. 98]. Figure 9 shows this phenomenon. Temperature changes parallels density fluctuations, though delayed by about two hours. The maximum atmospheric temperature occurs about 1630 and the minimum temperature digression is 12 hours later at 0430. This temperature effect is also altitude dependant.

To correct the nighttime exospheric temperature T_c for the diurnal variation the following is required:

$$\tau = H - 37 + 6\sin\,(H + 43) \qquad \text{(Eq 11)}$$

$$T_l = T_c \, (1 + 0.3\sin^{2.2}\theta)\,\left(1 + 0.3\left(\frac{\cos^{2.2}\eta - \sin^{2.2}\theta}{1 + 0.3\sin^{2.2}\theta}\right)\cos^{3.0}\left(\frac{\tau}{2}\right)\right) \qquad \text{(Eq 12)}$$

H being the local hour angle of the sun, and given:

$$\eta = \frac{1}{2}\left|\phi - \delta_s\right| \qquad \text{(Eq 13)}$$

$$\theta = \frac{1}{2}\left|\phi + \delta_s\right| \qquad \text{(Eq 14)}$$

with ϕ the latitude and δ_s the sun's declination.
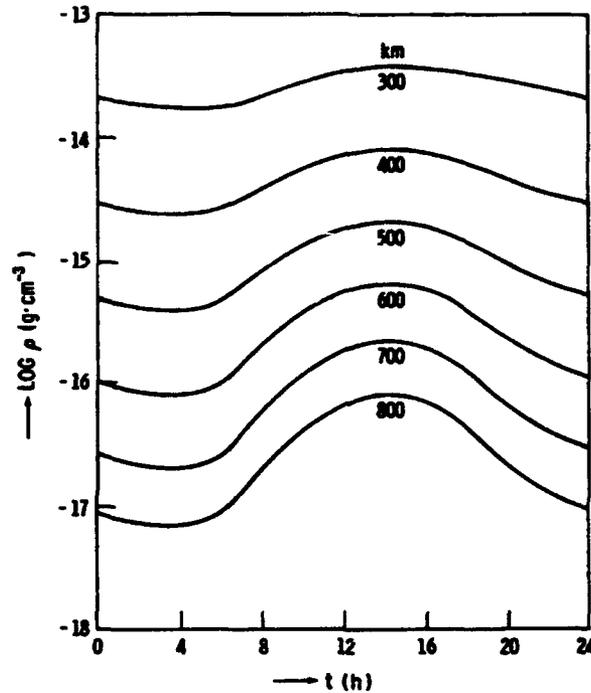

Figure 9: Diurnal Variation of Density [Ref. 11: p. 99]

3. Geomagnetic Effect

The sun constantly discharges a plasma (ionized gas) that hurls towards the earth at $400\frac{km}{s}$. When these charged particles interact with the earth's magnetic field a boundary is formed called the magnetopause, and complex currents are formed which flow about the earth. These currents induce a magnetic field. If this situation remained constant, this effect would not produce a perturbation. However, the sun discharges extremely fast moving

17

particles during its storms that cause radical fluctuations in the earth's current systems. These changes occur on a quick time scale, on the order of hours. The geomagnetic index records the fluctuations of the magnetic field on earth. It has been shown that due to these storms the geomagnetic index increases rapidly, and almost simultaneously the temperature and density of the auroral zones also increases. The increased temperature only propagates to the mid-latitudes, but the density increase propagates all the way to the low latitudes about eight hours later. Though the changes are of short duration, the density in the thermosphere may increase by an order of magnitude during a storm. The manner and method of the transport mechanism from the fast moving plasma to the rise in temperature and density is not yet well understood [Ref. 4: p. 286].

A typical magnetic storm is shown in Figure 10 which shows B-field measurements from a range of equatorial observatories. It is initialized by a sudden commencement (SC) that within minutes raises the magnetic field worldwide by $30 - 50nT$. This will last for $1 - 10$ hours, then the main part of the storm occurs with a decrease of $\approx 100nT$ below mean values of the magnetic field for $12 - 24$ hours. The third phase is a gradual return to the earth's nominal magnetic field value, typically $1 \cdot 10^{-4}T$. For comparison, the field strength near a small bar magnet is typically $1 \cdot 10^{-2}T$ [Ref. 12: p. 689]. Again, most of the geomagnetic heating is occurring in the auroral zones, so this effect mainly applies to polar orbiting satellites.

The equation:

$$\Delta T_g = 28Kp + 0.03e^{Kp} \qquad \text{(Eq 15)}$$

gives the change in temperature due to changes in Kp. Jacchia has a representation for this in ap (for ap description see page 23) given by:

18

$$\Delta T_g = 1.0 a_p + 100 \left(1 - e^{-0.08 a_p}\right) \qquad \text{(Eq 16)}$$

From here, ΔT_g is added to T_l to get the temperature T_∞, which is used to enter a lookup table to obtain the log of the atmospheric density, $log_{10} \rho_{l+g}$. The other entering argument is the specific altitude. This lookup table was created since changes in temperature change each gas constituent's concentration, and integrating over each constituent would take too much processing time for each revolution of the satellite. The lookup table allows for quick computation of the atmospheric density.
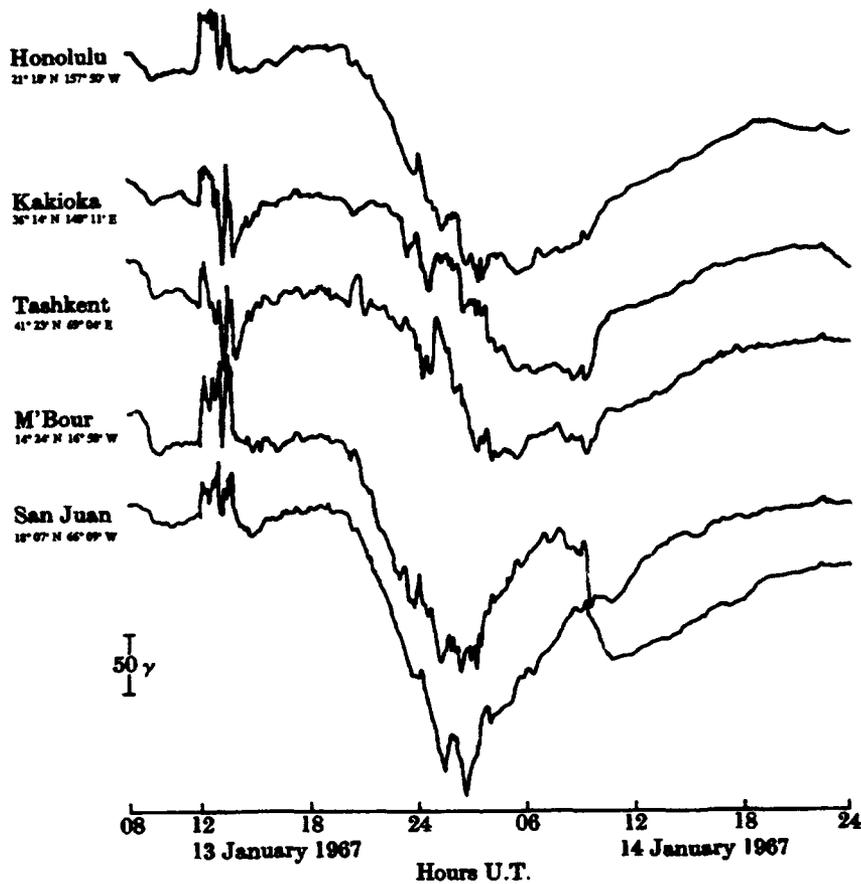
Figure 10: Geomagnetic Activity [Ref. 10: p. 557]

19

4. Semi-Annual Variation

There is a poorly understood semi-annual variation of density. The primary minimum occurs at the end of July and the primary maximum happens at the end of October; the secondary minimum is in mid January and the secondary maximum at the beginning of April. This effect is altitude dependant with the swings measuring 15% at 100 km, 25% at 200 km, and 200% from 500 km to 1000 km. [Ref. 4: p. 286]

Semi-annual variation adds its correction to the log of the density found previously. The following equations were used to generate another lookup table for this density correction:

$$\Delta log_{10}\rho_{sa} = \frac{f(z)}{g(t)} \qquad \text{(Eq 17)}$$

where

$$f(z) = (5.876 \cdot 10^{-7} z^{2.331} + 0.06328)\, e^{-(2868 \cdot 10^{-3} z)} \qquad \text{(Eq 18)}$$

$$g(t) = 0.02835 + 0.3817\,(1 + 0.4671\sin(2\pi\tau + 4.137))\sin(4\pi\tau + 4.259)$$

and

$$\tau = \Phi + 0.09544\left(\left(\frac{1}{2} + \frac{1}{2}\sin(2\pi\Phi + 6.035)\right)^{1.65} - \frac{1}{2}\right) \qquad \text{(Eq 19)}$$

with

$$\Phi = \frac{t - 36204}{365.2422} \qquad \text{(Eq 20)}$$

Here t is time in Modified Julian Days (= Julian Day - 2,400,000.5), and z is in kilometers. The log of the final actual thermospheric density is found by

$$log_{10}\rho = log_{10}\rho_{l+g} + \Delta log_{10}\rho_{sa} \qquad \text{(Eq 21)}$$

which can be solved for ρ and used in the equation for satellite drag (Eq. 1).

D. THE INDEXES

Indexes of geophysical phenomenon are published by the Journal of Geophysical Research each month for significant measurements. They are also available in digital form from dial-in bulletin boards [Ref. 6] or over the Internet [Ref. 7]. A brief summary of the pertinent indexes follows. All measurements are taken at Greenwich Mean Time (Zulu) designated by Z.

1. Solar Indexes

The F10.7 value is observed at 1400Z, 1700Z, and 2000Z at Penticton, Canada. It is located at 49° 30' N, 119° 35' W about 130 miles east of Vancouver, British Columbia. The 2000Z observation is taken as the world standard daily value. Approximately one and a half years ago F10.7 was measured at Ottowa, Canada, located at 45° 25' N, 75° 43' W. These measurements have been taken daily since 14 February, 1947 at 1700Z. Although now measured at Penticton, the solar flux is still sometimes referred to as Ottowa data.

During the search for actual F10.7 values, many F10.7 compilations turned up. It is imperative when comparing the forecast to the actual data, to use the actual received F10.7 values, and not the modified values. At the National Geophysical Data Center (NGDC) four separate F10.7 values were found on the database, all derivatives of the actual F10.7:

- *Observed Daily Solar Flux–* the uncorrected actual values

- *Adjusted Daily Solar Flux–* observed values corrected for an average Earth- Sun distance of 1 AU ($149.6 \cdot 10^6 km$)

- *Absolute Daily Solar Flux–* adjusted values corrected for antenna gain and reflected ground waves

• *Lenhart Data Values*– a compendium of various indexes, including Bartel's solar rotation number, 3-hour Kp, 3-hour Ap, Cp, and adjusted F10.7. Supposedly the same as the above adjusted values, yet does not appear to be.

A fifth set of actual F10.7 and Ap values was found at A.F. Space Weather Detachment 2, Onizuka AFB.

2. Magnetic Indexes

Measuring deviations of the earth magnetic field is accomplished by arranging three magnetometers into an orthonormal configuration: X pointing to geomagnetic north, Y pointing geomagnetic east, and Z pointing downward. The actual deviations are registered in the H, D, I, coordinate system where: H is the horizontal direction, D is the declination from north (to the eastward being positive), and I the inclination or dip angle (into the earth being positive). These measurements are taken constantly worldwide by a
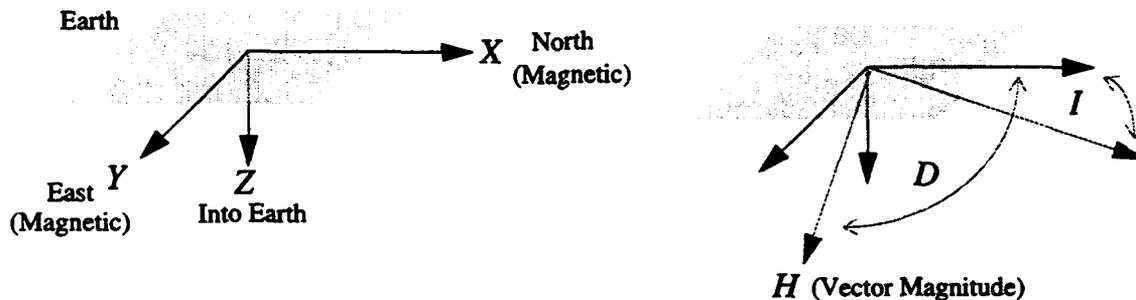
series of magnetic observatories, and are measured in nT, otherwise known as γ. The largest deviation over a three hour period in any of the three directions is transcribed as the maximum range in γ, r_γ, which is then converted into a K value using the following semi-logarithmic chart:

r_γ	0	5	10	20	40	70	120	200	300	500
K	0	1	2	3	4	5	6	7	8	9

Each station modifies its K reading to account for local and seasonal variations, obtaining a standardized value Ks. This is a finer scale than K by using one of three modifiers: –, o, and + to get incremental adjustments of $\frac{1}{3}$. For example, a K between 4.33 to 4.66 would become a 4+; a K of 4.66 to 5.00 would become a 5–; and a K of 5.00 to 5.33 would become a 5_0. Kp is then obtained by the averaging the Ks values of twelve observatories placed worldwide. Each Kp therefore is an indicator over a thee hour period of the worldwide geomagnetic activity. The three hour periods commence at 0000Z; consequently there are eight Kp's calculated per day. [Ref. 10: pp. 552-556]

The A index is a linearization of the K index using the following chart:

Kp 0_0 0_+ 1. 1_0 1_+ 2. 2_0 2_+ 3. 3_0 3_+ 4. 4_0 4_+ 5. 5_0 5_+ 6. 6_0 6_+ 7. 7_0 7_+ 8. 8_0 8_+ 9. 9_0

ap 0 2 3 4 5 6 7 9 12 15 18 22 27 32 39 48 56 67 80 94 111 132 154 179 207 236 300 400

The planetary average Ap is found by averaging the ap's over a 24 hour period:

$$Ap = \sum_{i=1}^{8} \frac{ap_i}{8} \qquad \text{(Eq 22)}$$

It is seen that the parameter Ap has gone through quite a few mathematical manipulations, in addition to the fact that for an index given daily, it is characterizing an event that occurs over the course of a few hours. [Ref. 10: pp. 552-556]

Other indexes are the AE index used in high latitude areas to measure the auroral electrojet, and the D_{st} index used in the low latitudes.

E. LIFETIME 4.1

The Lifetime 4.1 program from the Aerospace Corporation [Ref. 16] provided the data for the orbital propagation analysis. The program was used to test the extent of errors in forecasting F10.7 and Ap as related to the numbering of satellite revolutions and height

23

of perigee. This program provides ease of use, portability, and availability of either the

Jacchia '71 or Jacchia/Walker '64 dynamic atmosphere model. Lifetime can run on the *86

series computers from Intel. It is a menu-based system that also allows for ease of use. The

output available from this program is a columnar text file listing:

- the number of days into the propagation routine

- the corresponding number of revolutions completed by the satellite

- the height of perigee in kilometers

- the height of apogee in kilometers

- the current eccentricity

Below the user-defined Runga-Kutta integration starting altitude it only gives:

- the number of days into the propagation routine

- the spacecraft current altitude

Additionally, there is graphical output from the Lifetime 4.1 program including:

- charting the perigee and apogee altitudes in *km* over time

- global plotting of satellite groundtrack, including initial debris point, center of mass impact point, and the final debris point

- charting of spacecraft altitude vs. time to impact, with the aforementioned three parameters labeled

Sample graphical outputs, Figures 11 & 12, are provided for reference though graphical

data was not used in this study.

PERIGEE/APOGEE DECAY HISTORY
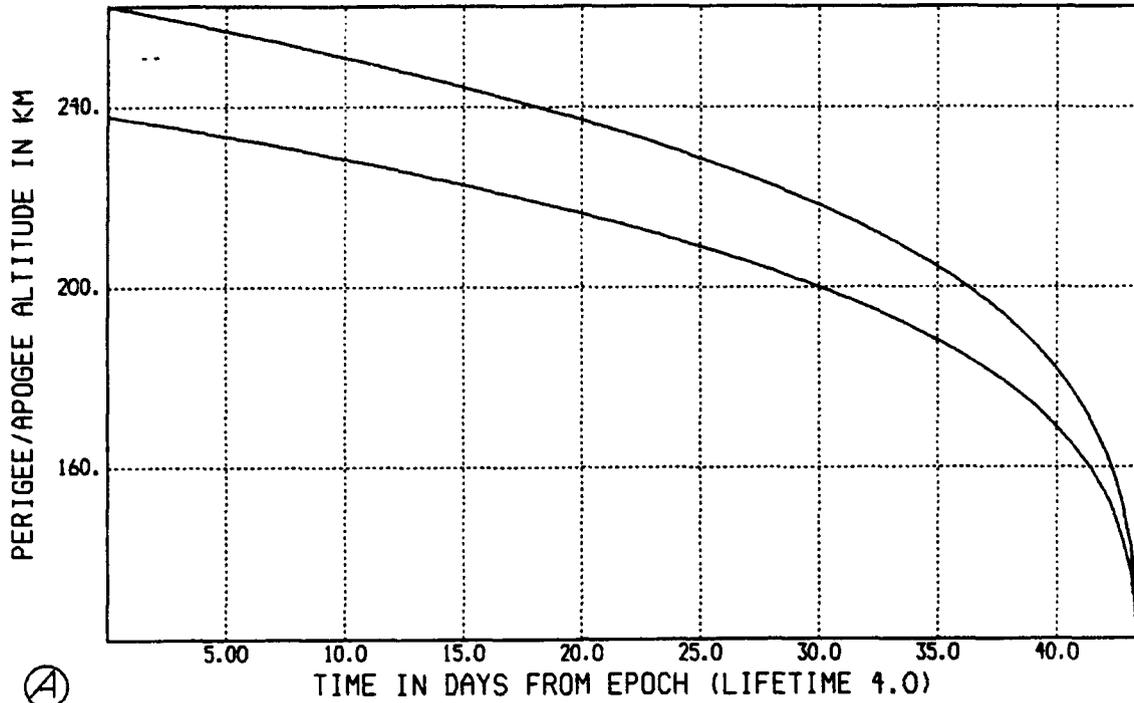
Figure 11: Lifetime 4.1 Sample Output [Ref. 16]

LIFETIME: GROUNDTRACK/DEBRIS IMPACT AREA
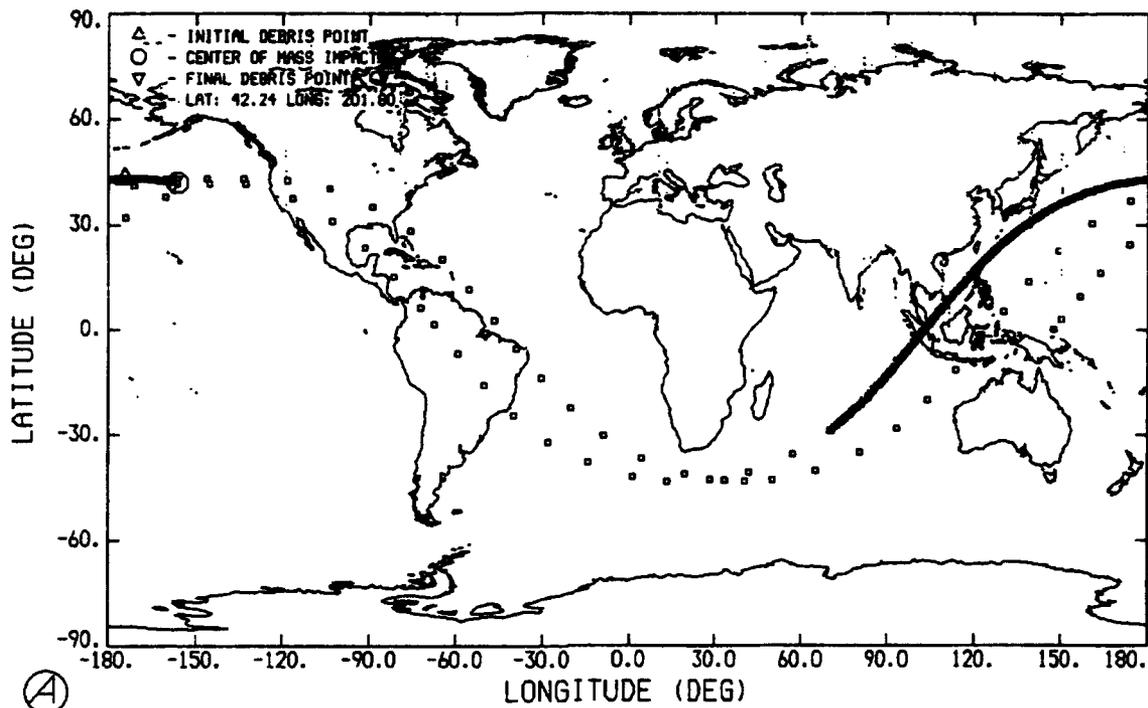
LIFETIME: VEHICLE ALTITUDE DECAY
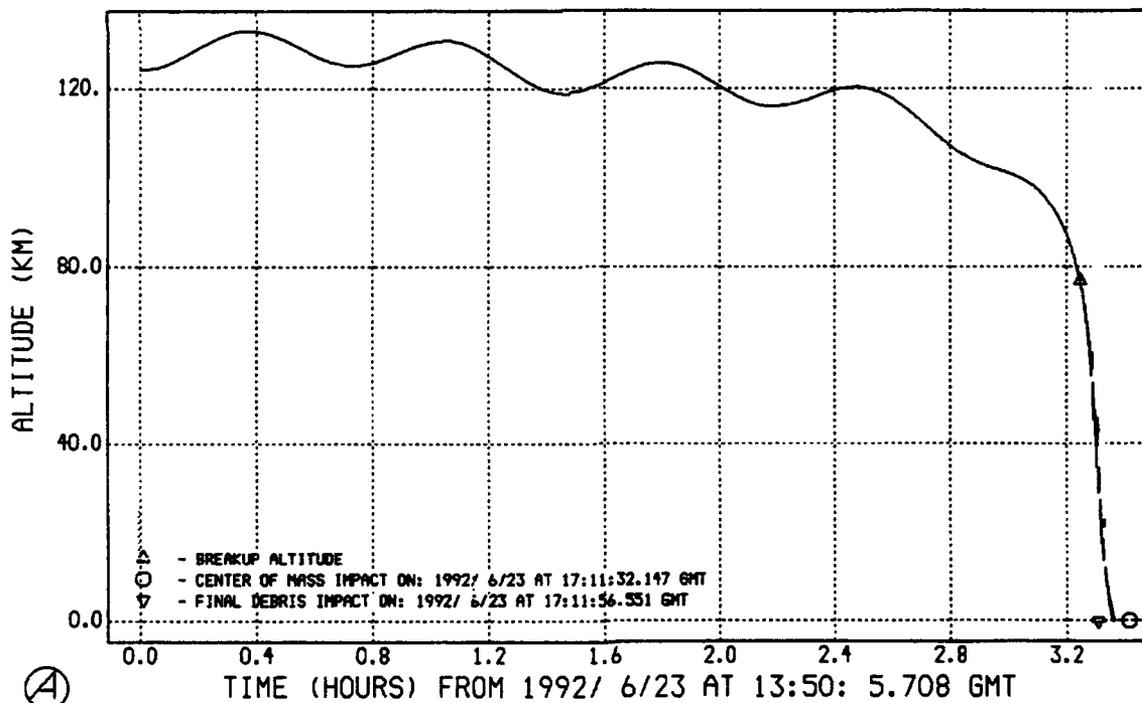
Figure 12: Lifetime 4.1 Sample Output (cont.) [Ref. 16]

III. DATA PROCESSING

This next section describes the methods of data collection, manipulation and analysis efforts. All work was done on either a 68030 Macintosh or a 80386 PC. The surveyed data set was compiled daily from 18 December, 1992 until 21 October, 1993, a total of 308 days.

A. DATA COLLECTION

1. F10.7 and Ap

The predicted F10.7 and Ap values were collected via message traffic from the Air Force Space Forecast Center, Falcon AFB, Colorado. This daily message consists of predicted F10.7 and Ap values for the coming 45 days, as shown in Figure 13.

```
R181931                    *****************************
   ROUTINE                 *  U N C L A S S I F I E D  *
                           *****************************


45-DAY AP FORECAST
13NOV93 012 14NOV93 010 15NOV93 007 16NOV93 007 17NOV93 007
18NOV93 012 19NOV93 010 20NOV93 010 21NOV93 015 22NOV93 015
23NOV93 030 24NOV93 020 25NOV93 010 26NOV93 010 27NOV93 010
28NOV93 010 29NOV93 010 30NOV93 012 01DEC93 015 02DEC93 035
03DEC93 030 04DEC93 020 05DEC93 015 06DEC93 010 07DEC93 010
08DEC93 010 09DEC93 010 10DEC93 010 11DEC93 010 12DEC93 010
13DEC93 010 14DEC93 010 15DEC93 010 16DEC93 010 17DEC93 010
18DEC93 015 19DEC93 015 20DEC93 025 21DEC93 015 22DEC93 010
23DEC93 010 24DEC93 010 25DEC93 010 26DEC93 010 27DEC93 010
45-DAY F10.7 CM FLUX FORECAST
13NOV93 090 14NOV93 090 15NOV93 090 16NOV93 090 17NOV93 095
18NOV93 095 19NOV93 095 20NOV93 090 21NOV93 090 22NOV93 090
23NOV93 090 24NOV93 090 25NOV93 095 26NOV93 095 27NOV93 095
28NOV93 095 29NOV93 095 30NOV93 090 01DEC93 090 02DEC93 090
03DEC93 090 04DEC93 090 05DEC93 085 06DEC93 085 07DEC93 085
08DEC93 085 09DEC93 085 10DEC93 080 11DEC93 080 12DEC93 080
13DEC93 085 14DEC93 085 15DEC93 085 16DEC93 085 17DEC93 090
18DEC93 090 19DEC93 090 20DEC93 090 21DEC93 090 22DEC93 090
23DEC93 090 24DEC93 090 25DEC93 085 26DEC93 085 27DEC93 090
BT
*5455
```

Figure 13: Typical Daily F10.7 & Ap Forecast [Ref. 17]

27

These values were entered daily by hand into a spreadsheet program for analysis, a total of over 28,000 individual cell entries. These messages may be obtained by calling the Space Forecast Center (AV 560-6206) and placing the command onto the routing list.

The actual F10.7 and Ap values were obtained from records kept by the A.F. Space Weather Group at Onizuka AFB. These records were also on hardcopy and had to be entered by hand. The F10.7 values used were the actual daily measurements. The Ap values used were the 2400Z readings. These values were used because the online database at the National Geophysical Data Center (NGDC) did not appear reliable. Specifically, although the actual values given to the author by E. Erwin at NGDC matched the values logged by the Onizuka personnel, the values for 1992 F10.7 adjusted, found in the "Ottawa" directory did not match the 1992 adjusted values located in the "Lenhart" file. Therefore the NGDC data was discounted in favor of the Onizuka data.

2. Lifetime 4.1 Data

The basic procedure was to create a reference orbit with all values known and assumed to be true. It was propagated for 45 days and the ending orbital revolution number and final perigee altitude noted. In all cases the calculation was stopped at or above $100km$ to inhibit the engagement of the Runga-Kutta integration routine. Reference orbits were generated for every $25km$ from $150km$ to $450km$. From each reference orbit only changes in F10.7 were allowed, evenly distributed over typical maximum and minimum F10.7 values of 70 and 220. The current F10.7 average calculated from the actual data set was found to be 113, so the F10.7 values we set to 70, 91.5, 113, 134.5, 156, 177.5 199, and 220.5.

The Lifetime 4.1 model allows for changes in the ballistic coefficient through differential correction. This feature is used to allow the model to better match actual re-entry trajectories. Simply put, this feature absorbs all errors in actual satellite position, whatever the source, and allows for a better curve fit. This survey, however, is not out to determine past accuracies of actual vs. predicted satellite re-entry trajectories, but to give readers a tangible feeling for how errors predicting F10.7 can radically affect projected revolution numbers and altitudes of satellite orbits. Hence the differential correction feature was disabled because it is assumed that all other modeled factors are accurately known.

All the satellite orbits were initiated with the following parameters as required by the Lifetime 4.1 model:

- start date– January 1, 1993 @ 01 hours 01 minutes 01 seconds
- orbital elements– set to mean
- semi-major axis– varied between $6528km$ and $6828km$ by $25km$
- eccentricity– varied between .0001 and .0010 by .0003
- inclination– set to 45°
- right ascension– 1°
- argument of perigee– 1°
- true anomaly– 1°
- inverse ballistic coefficient– $66.6667\frac{cm^2}{kg} = 150\frac{kg}{m^2} = 30.722\frac{lb}{ft^2}$
- variable ballistic coefficient caused by solar panels– not used
- the Jacchia '71 model was used for atmosphere above $90km$
- the 1962 standard atmosphere was employed below $90km$

Instead of using the program's generated F10.7 and Ap values, the Ap was set to 8 for all evolutions (though not the actual calculated mean of 13.5, it is used by disregarding the outliers), and the F10.7 varied per each run as previously mentioned. (It is noted here that

a user specified F10.7 and Ap value can be entered into Lifetime 4.1 on a daily basis using a vectored input file. This would be a good way to test the actual values of F10.7 and Ap vs. the predicted values over the entire time series, for both various altitudes and predicted days out). The linear rate of change was not used, as comparison to the generated reference with known deviation was required. No orbital sustenance was employed, but the J_3 perturbation was used for a more realistic output. The model propagated in step sizes of 1 revolution, until the user specified integration altitude was reached. For this project the beginning of the thermosphere at $100km$ was selected. The end of the propagation routine was set to the spacecraft breakup altitude, $77.784km$. Two reasons for this choice are given. First, since F10.7 has little affect on altitudes lower than $100km$, it was not necessary to continue analysis beyond this point. Secondly, spacecraft dynamics during the re-entry phase is not know very accurately, modeling the ballistic coefficient itself during this phase is a topic unto itself. This study concerns itself with errors in F10.7 and Ap, and their effects upon propagation routines until the spacecraft breakup altitude.

The values for number of completed revolutions and the height of perigee were copied into a spreadsheet for analysis.

B. MANIPULATION OF DATA

The forecast data comes in a format listing future predicted values from the current day, not in a format showing the predicted values generated for *this particular day*, from the past 45 days of predictions. In order to view the changes over time of the forecasted values, the daily predicted values were reformatted into a table, listing by day, each predicted value given for it during the last 45 days. It is changes in this data that affect the operational user.

Extensive use of self-written Excel macros were used to manipulate the data sets into a usable form with the actual value given on the left, and the predicted values shown for each previous day, back for 45 days, on the right. Figure 14 shows the format. Once in this state simple column manipulations were done to obtain the final data set: determining the error of each forecast. Error was defined as "forecasted value - actual value".

	A	B	C	D	E	F	G	H	I	J
		F10.7	1	2	3	4	5	6	7	8
2	18-Dec-92	150	#N/A	#N/A	#N/A	#N/A	#N/A	#N/A	#N/A	#N/A
3	19-Dec-92	147	145	#N/A	#N/A	#*#	#N/A	#N/A	#N/A	#N/A
4	20-Dec-92	148	150	140	#N/A	#N/A	#N/A	#N/A	#N/A	#N/A
5	21-Dec-92	145	155	155	135	#N/A	#N/A	#N/A	#N/A	#N/A
6	22-Dec-92	142	150	160	165	130	#N/A	#N/A	#N/A	#N/A
7	23-Dec-92	144	150	150	165	165	125	#N/A	#N/A	#N/A
8	24-Dec-92	136	140	155	145	160	160	120	#N/A	#N/A
9	25-Dec-92	136	##	##	##	##	##	##	##	##
10	26-Dec-92	131	#N/A	140	135	150	135	150	145	120
11	27-Dec-92	125	130	#N/A	135	130	145	130	145	120

Figure 14: Date, Actual F10.7 Value, & Predicted Values 1 to 45 Days-Out

C. GENERATION OF STATISTICAL DATA

To compute the accuracy of the forecasted F10.7 and Ap, statistical values were calculated using Excel on a Macintosh computer. Each day is an array of 45 values for errors in F10.7, and another set of 45 values for errors in Ap. The study resulted in a matrix with 309 rows by 90 columns. Manipulation of this data produced the following statistical information:

1. Mean

The average value of a series defined as

$$\bar{y} = \frac{\sum_{i=1}^{n} y_i}{n} \qquad \text{(Eq 23)}$$

where n is the number of data points, and y_i is the value of each data point.

2. Standard Deviation

Gives the range, or extent, of the data values spread out from the mean, defined as

$$\sigma = \sqrt{\frac{n \sum_{i=1}^{n} y_i^2 - \left(\sum_{i=1}^{n} y_i\right)^2}{n(n-1)}} \qquad \text{(Eq 24)}$$

One standard deviation contains approximately 68% of the data, two standard deviations will contain approximately 95% of the data, and three standard deviations will contain approximately 100% of the data.

3. Kurtosis

Defines the peakness or flatness of the distribution as compared to a normal distribution. Positive kurtosis and negative kurtosis are illustrated below:

$k = 3$ $k < 3$ $k > 3$
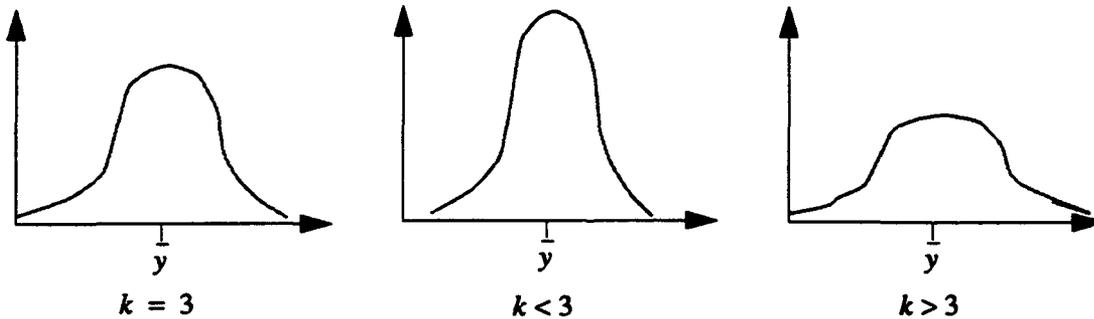
It is defined as

$$k = \left[\frac{n(n+1)}{(n-1)(n-2)(n-3)} \sum_{i=1}^{n} \left(\frac{y_i - \bar{y}}{\sigma}\right)^4 \right] - \frac{3(n-1)^2}{(n-2)(n-3)} \qquad \text{(Eq 25)}$$

A normal population will have $k = 3$; distributions with longer, heavier tails will have $k > 3$, distributions with smaller tails will have $k < 3$.

4. Skewness

Determines the degree of a distribution's asymmetry about the mean. Positive skewness and negative skewness are illustrated below:

$$s = 0 \qquad\qquad s > 0 \qquad\qquad s < 0$$
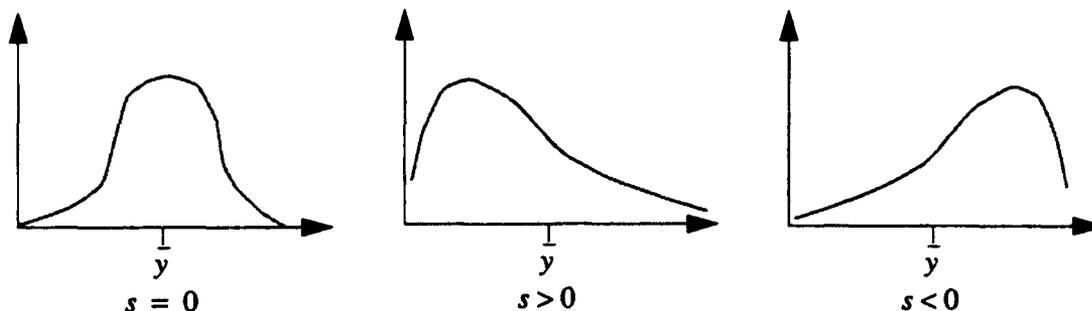
It is defined as

$$s = \frac{n}{(n-1)\,(n-2)} \sum_{i=1}^{n} \left(\frac{y_i - \bar{y}}{\sigma}\right)^3 \qquad \text{(Eq 26)}$$

and can be used to determine if a distribution is symmetrical.

D. ERROR ANALYSIS OF DATA ENTRY

Errors in data entry was checked on a statistical basis. Every day ending in 8 (i.e. the 8th, 18th, and 28th of each month) from the first data set (Dec 18, 1992) to the last data set (Oct 21, 1993) was pulled from the main body of data. For each of these days, the fifth column's forecasted values for F10.7 and Ap were checked against the original hardcopy document. All cases were found to be correct, and it is assumed that the transcription from hardcopy to computer was made without errors for the entire data set.

IV. RESULTS

The following F10.7 and Ap charts and data analysis relies on the 308x90 data matrix previously mentioned. The label "days-out" refers to how many days away from the actual date the forecast was made. For example, an actual F10.7 value of 143 taken on 9 March, 1993, had a predicted value of 150 made on the 8th of March (1 day-out) and a predicted value of 140 made on the 28th of January (40 days-out).

Errors in F10.7 and Ap are defined as actual values minus the forecasted values. Hence an error of -5 would indicate that the actual value was lower by five from the forecasted value, an over-forecast.

A. F10.7

The data gathered for this study spans 308 days. The actual F10.7 values are shown in Figure 15. From this graph we notice the 27 day solar cycle, as evidenced by the symmetrical occurrence of peaks and valleys. This 27 day cycle is the mean rotation of the sun about its axis (the equatorial regions rotate once every 24.9 days, polar regions rotate once every 31.5 days) [Ref. 1: p. 15]. Also apparent is the approach of the solar minimum, as evidenced by the overall downward trend. It is also noted that departures occur, hence the predictability problem. Statistics from the actual data:

- Mean- 113.4
- Standard deviation- 22.2
- Skewness- 0.59
- Kurtosis- 0.29

Figure 16 is a histogram of the actual F10.7 flux values. The bins are arranged by a difference of 3. We see that the distribution is not normal and has more than a few outliers,

though only in one direction (larger values). Figure 17 shows how many data points were involved for each predicted day-out. Obviously, there is no 1 to 45th day predicted data point for the first day in the study. Hence there are more data points for the 1 day predictions than for the 45 day predictions. However, with all days-out having over 220 data points, sample sizing is adequate. The line is not linear due to dropout dates when no forecast message was received.

Figure 18 shows the mean and standard deviation of the forecasted errors. We note that one day-out, the mean error is approximately zero. The errors slip from there, fairly steadily, down to about -7 for the 45 day-out prediction. This indicates that the predicted F10.7 values are slightly over-forecasted, with an increased magnitude as time draws backward. The standard deviation show a parabolic expansion from one day-out to seven days-out; effectively doubling the range of forecasted errors in one week's time. It then maintains a value of 19 for the rest of the predicted period, except for a slight increase at the end. This shows two things. First, that beyond the seven days-out, the range of errors does not change much at all. Secondly, within seven days-out the forecasting becomes much improved, with one day-out being the best forecast.

Figure 19 shows the skewness of the forecasted errors. We see that the forecasted period is distinctly broken up at almost exactly the half way point, 24 days-out, into two periods. Both begin and end with the errors having a symmetric distribution about the mean. The first half has an error distribution that is positively skewed, meaning there is a longer tail of errors out at the larger (under-forecasted) error values. The second half, for 24 to 45 days-out, is negatively skewed, meaning there is a longer tail of errors at the smaller (over-forecasted) values. A reason for this dichotomy is not understood, though it

is interesting to note that the 27 day-out point (which fits the 27 day solar cycle) also has a symmetric distribution of over-forecasts and under-forecasts.

Figure 20 shows the F10.7 kurtosis. We see that nowhere are the errors symmetrically distributed; however one and eight days-out get close. The error distributions are less peaked (shorter tail) than a normal distribution, meaning they are closer to the mean error.

Figures 21 through 26 show histograms for the errors made; each chart is for a range of errors as specified. It is seen that there are frequently low valued errors ($0 \leq x < 10$) made for one to seven days-out. During the same time period, there is a low frequency of large errors ($x \geq 20$). This is as expected. Conversely, the frequency of errors for each category keep relatively the same between the 17 day-out and the 45 day-out period. Interestingly, the large magnitude errors ($x > 60$) were all made exclusively during a short one week period, 5 to 13 days-out. No errors of this magnitude occur at any other time.

It appears that the forecasted values for F10.7 are quite good from 1 to 7 days-out. There is a general tendency to over-forecast, especially at the longer days-out. There exists a band during the second week out where the largest errors are made. The overall range of errors after the first week out is almost a constant over the 38 day period.
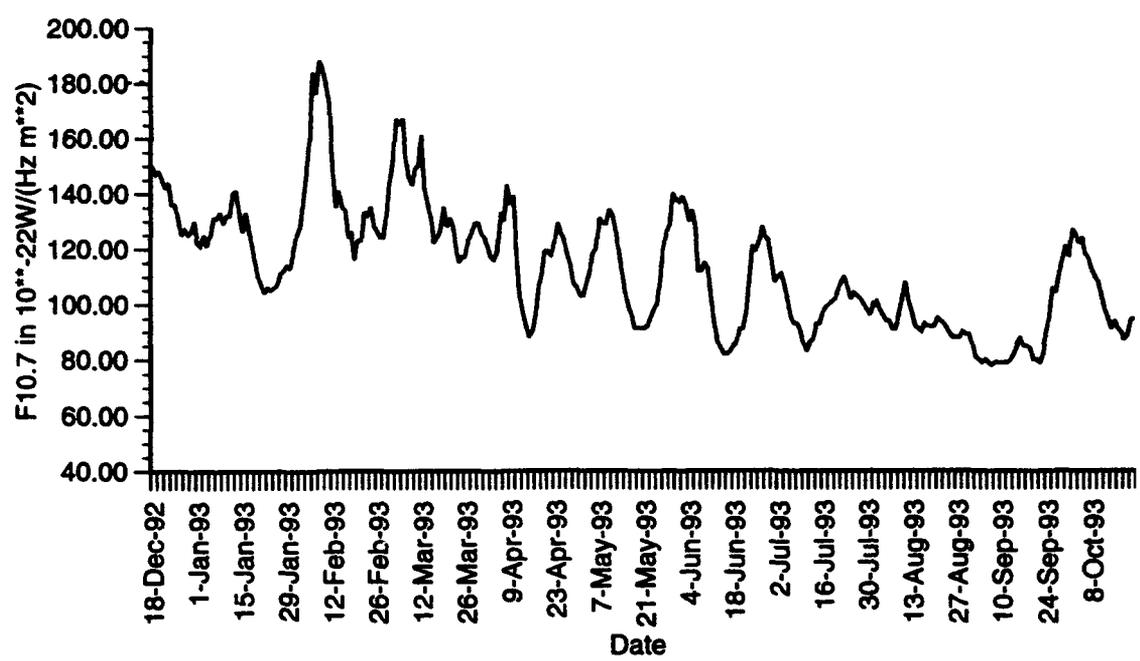
Figure 15: Actual F10.7 Flux

value on left < total F10.7 counts in bin ≤ value on right
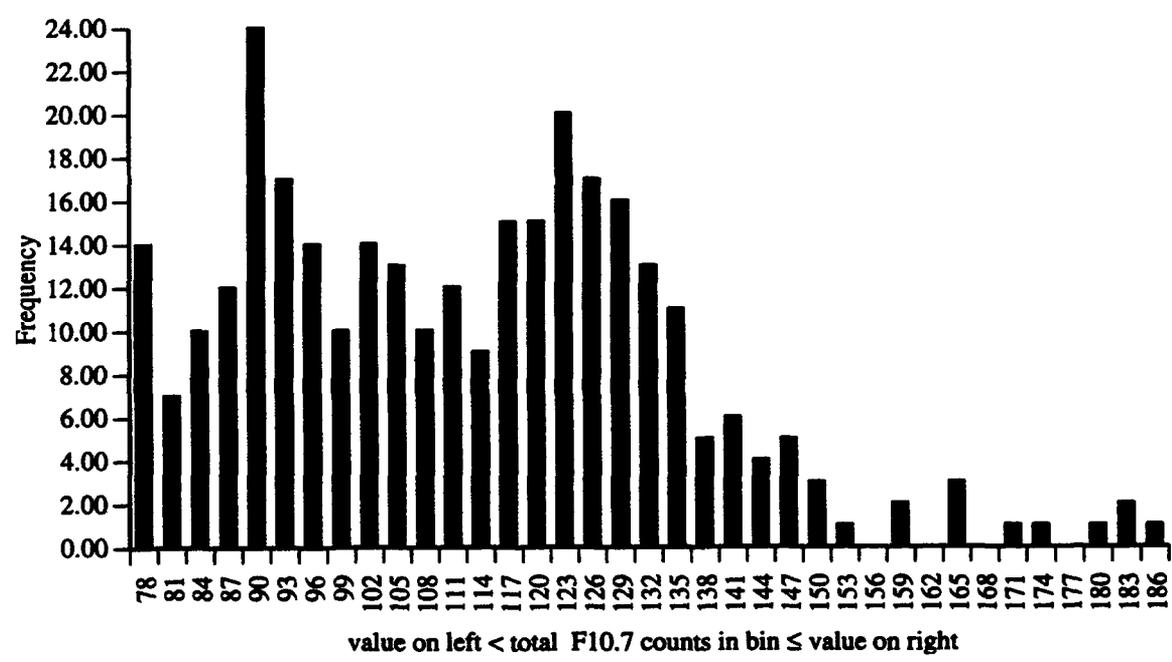
Figure 16: Actual F10.7 Flux Histogram
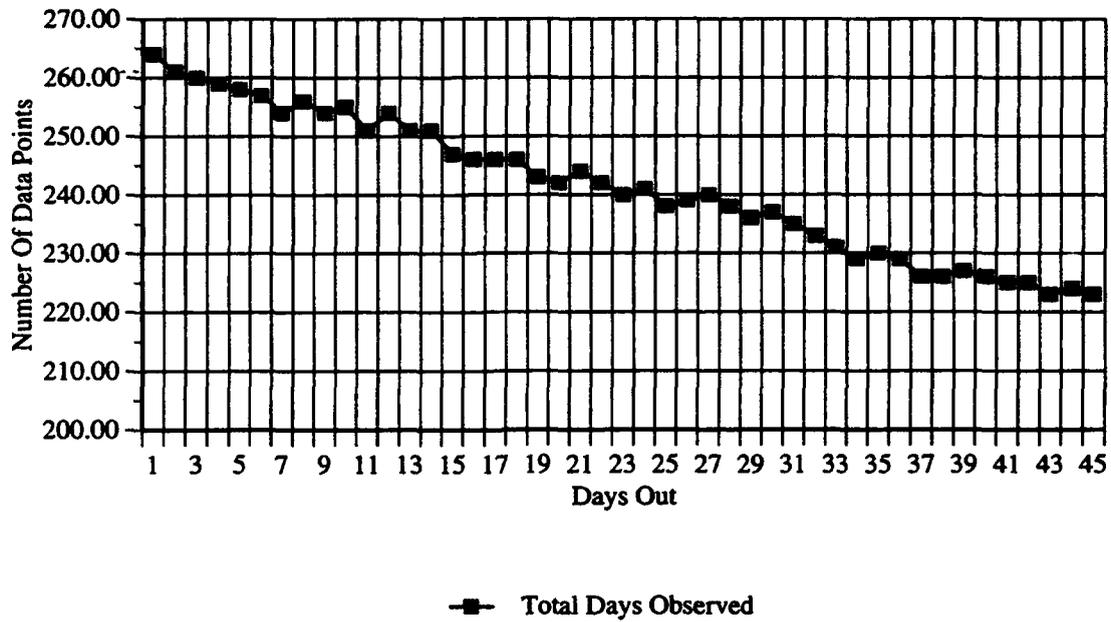
Figure 17: Number of F10.7 Flux Data Points
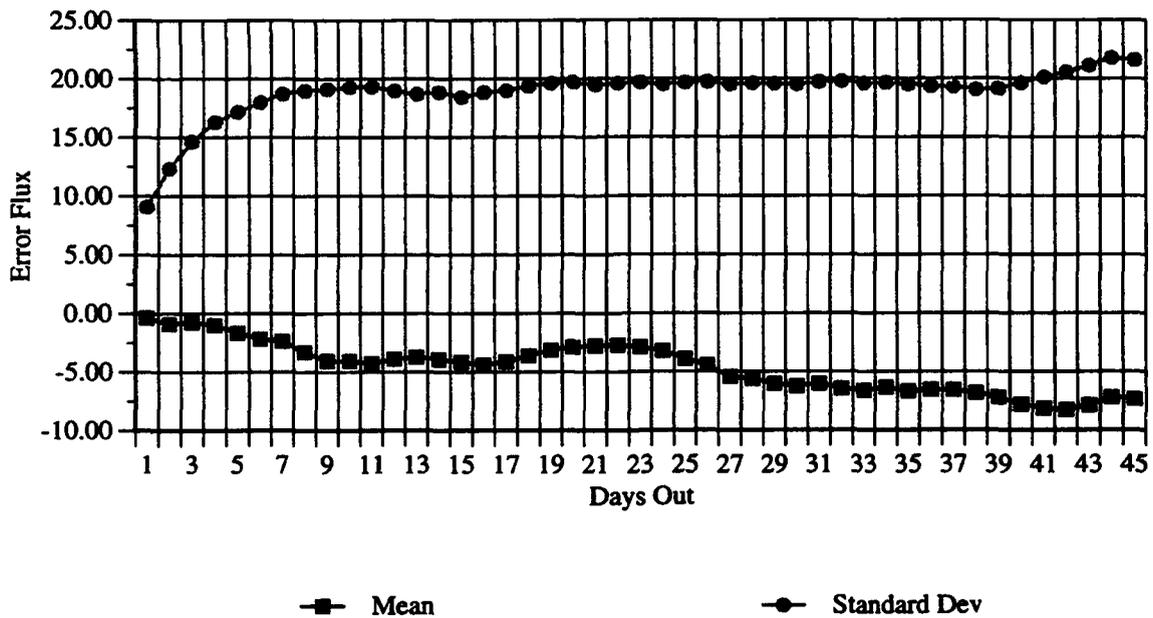
Figure 18: F10.7 Error Statistics
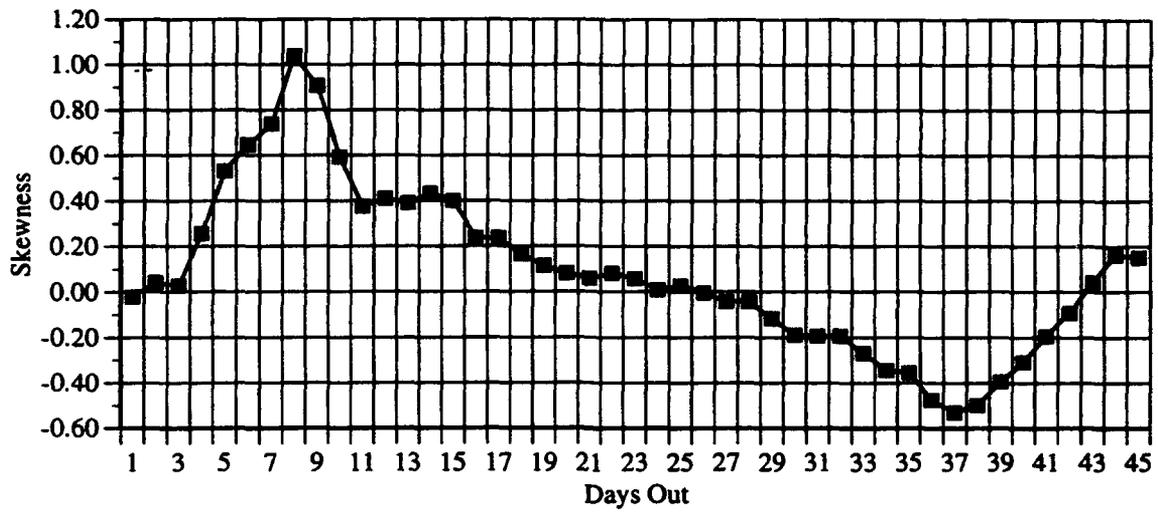
Figure 19: F10.7 Error Skewness
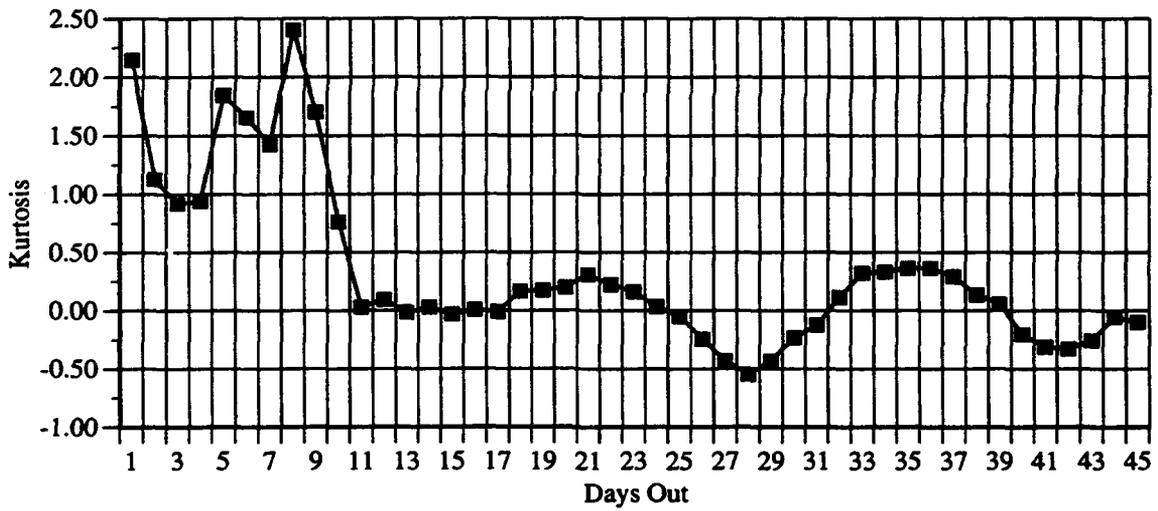
Figure 20: F10.7 Error Kurtosis
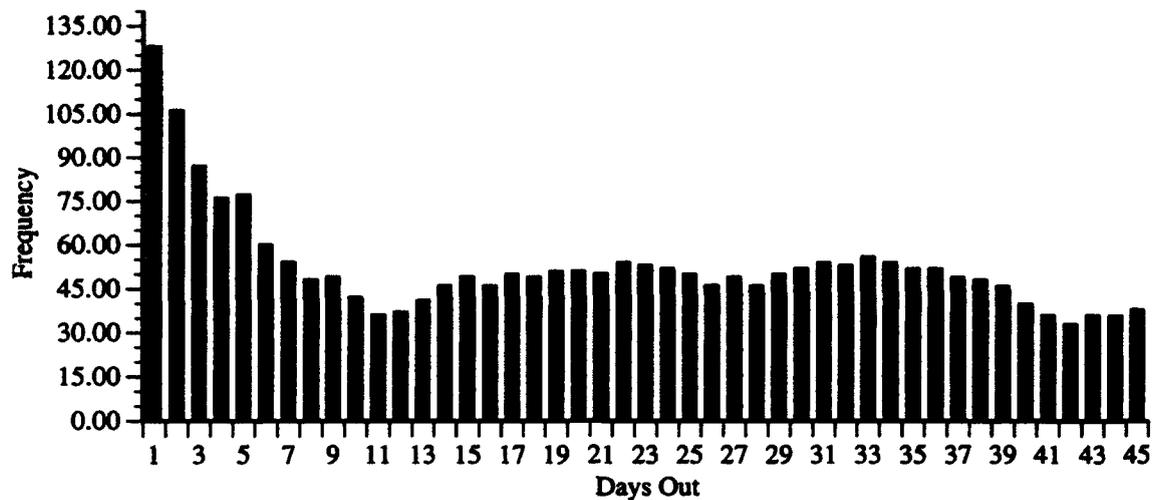
Figure 21: Number of F10.7 Errors $0 \leq x < 5$
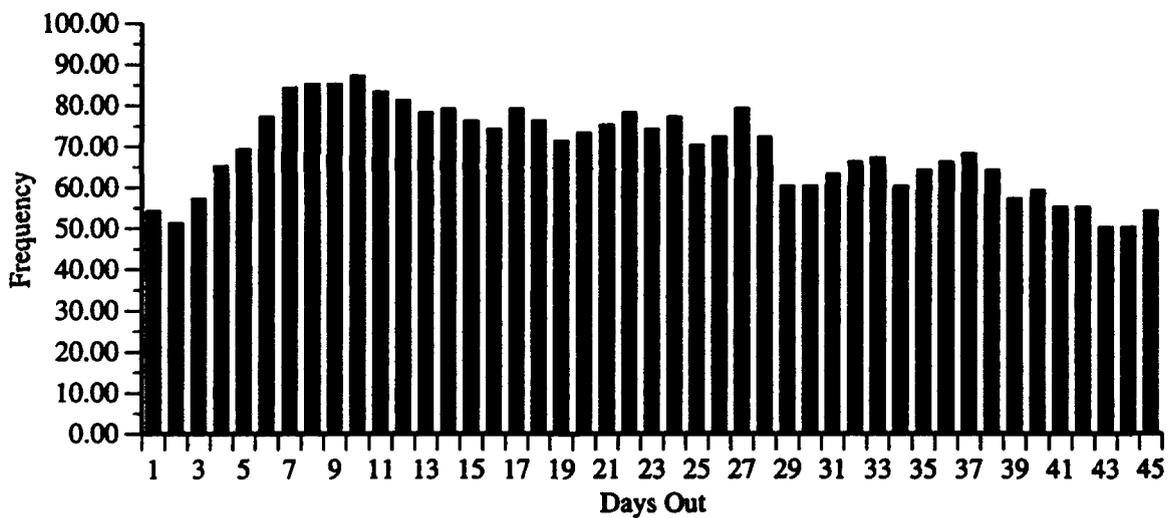
Figure 22: Number of F10.7 Errors $5 \leq x < 10$
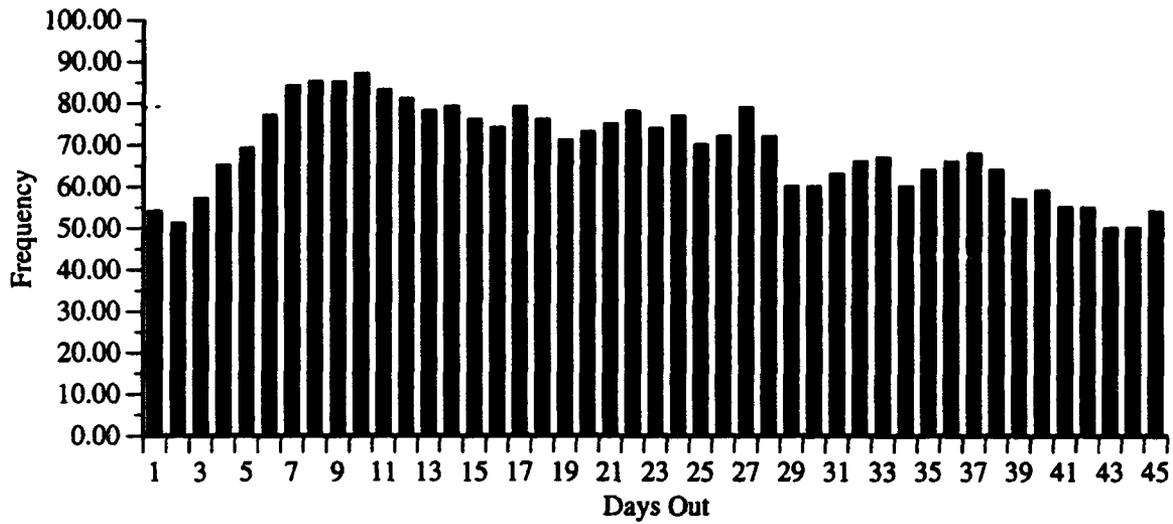
Figure 23: Number of F10.7 Errors 10 ≤ x < 20
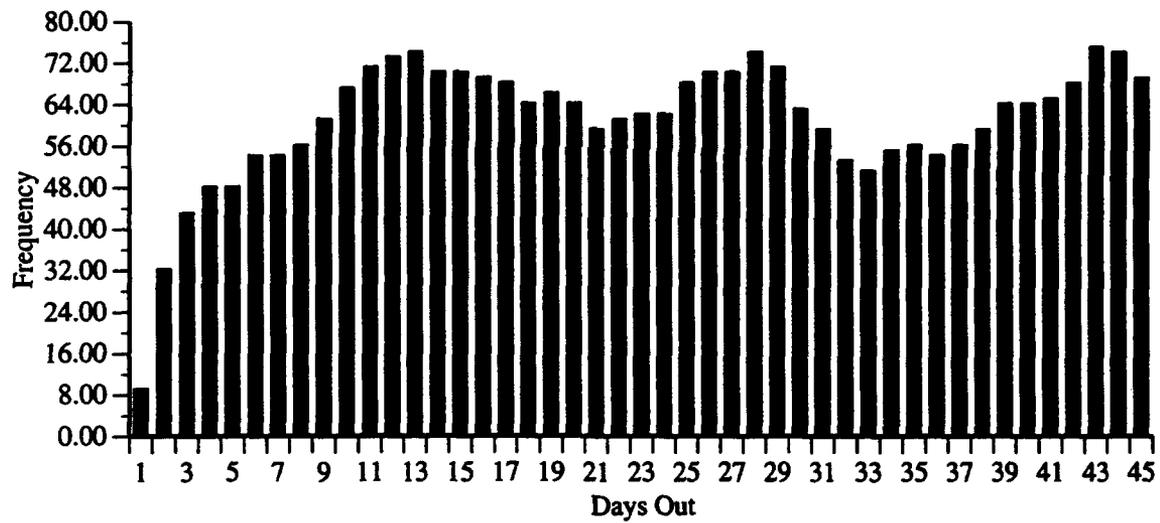
Figure 24: Number of F10.7 Errors 20 ≤ x < 40

41
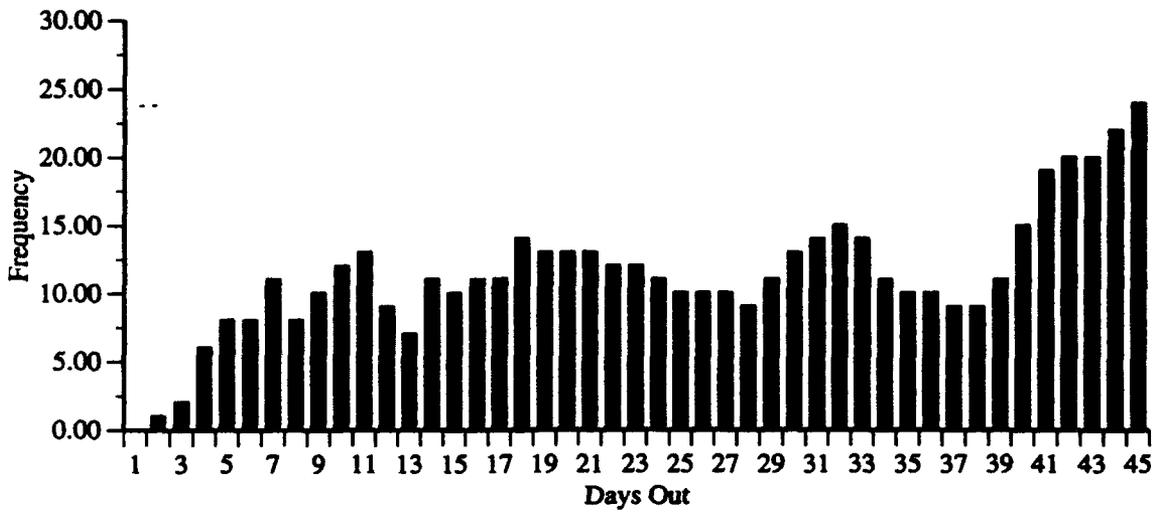
Figure 25: Number of F10.7 Errors 40 ≤ x < 60
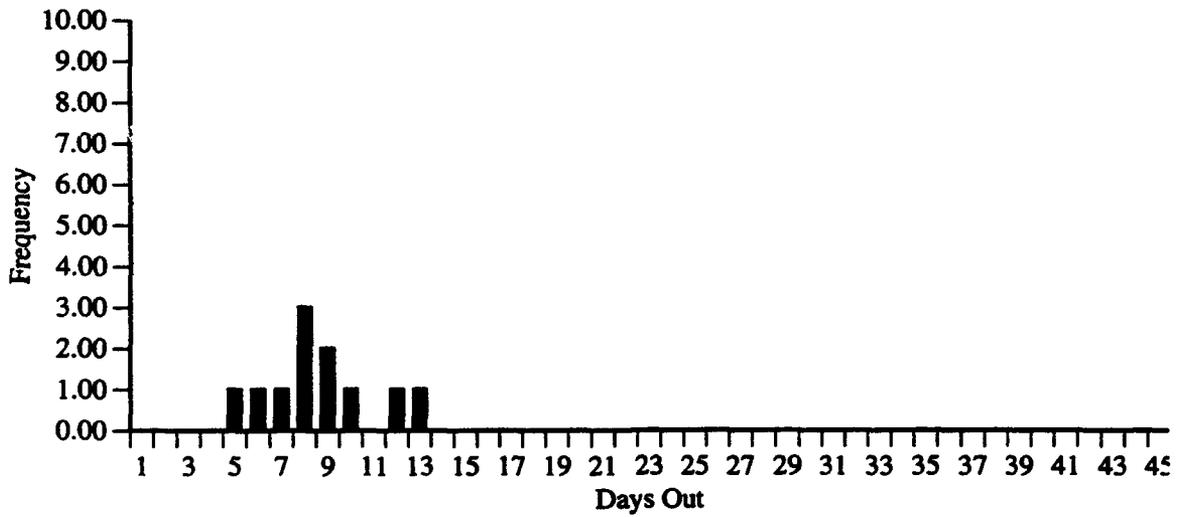
Figure 26: Number of F10.7 Errors 60 ≤ x

42

B. Ap

The actual Ap values are shown in Figure 27. Clearly, there is a large range of fluctuation in this data: Ap values are spread over two magnitudes. Also seen, though not understood by this author, is an apparent 10 day cycle of the peaks. Even though Ap is a linearization of the K index (which is a logarithmic scale of the geomagnetic field; see page 22), it still shows extreme ranges obtained on a fairly frequent basis. Looking at Figure 28, a histogram of the actual Ap values, we see that is reminiscent of the Planck blackbody radiation curve, and is not a normal distribution. Even if the outliers were removed, it would still not have a normal distribution. Statistics from the actual data:

- Mean- 13.9
- Standard deviation- 12.5
- Skewness- 3.41
- Kurtosis- 17.3

Figure 29 shows the total number of data points for each day-out. Again it is not strictly linear as previously explained.

Figure 30 is the mean and standard deviation of the errors in forecasted values. Here it is noted that the one day-out mean error is -2 (an over-forecast) and steadily climbs to just under 1 (an under-forecast) on the sixth day-out. For the rest of the forecast range it remains around this value. It is also noted that the standard deviation is largest at one day-out and drops until four days-out. This is a radical departure from the F10.7 statistics (see Figure 18); it shows that the forecasted Ap values actually get worse with time from about six days-out until one day-out. Also significant is the fact that the standard deviation is practically constant throughout the entire 45 day period. This implies that the Ap

forecasting never gets better over time, and as seen, actually deteriorates within seven days-out of the actual reading.

Figure 31 shows the skewness of the Ap data. This shows that the errors in forecasting Ap are never symmetric. With an exception for the first and last day-out, the skewness is approximately 2.75 throughout. This means that each day-out has the same propensity for more values in the positive (under-forecasting). This implies there are too few forecasts made of large Ap values with respect to the actual occurrences.

Figure 32 show the Ap kurtosis. This is again a radical departure from the F10.7 statistics. The rather large positive values indicate a large tail, indicating the errors are not located relatively close to the mean. This is because forecasting a large Ap value is seldom accomplished, inherently creating a large positive error, and hence the tail in the distribution.

Figures 33 through 38 show histograms of the errors. It is seen that with one exception, the errors generated are generally uniform throughout the entire forecasted period, whether from 1 day-out or from 45 days-out. This is not expected, as one would hope that with time, larger errors would decrease and smaller errors increase, snowing some form of skill. This is evident with the F10.7 data. The only exception is Figure 34, where a trend to make more errors in the 5 to 10 range, as time approached the actual date, begins to appear.
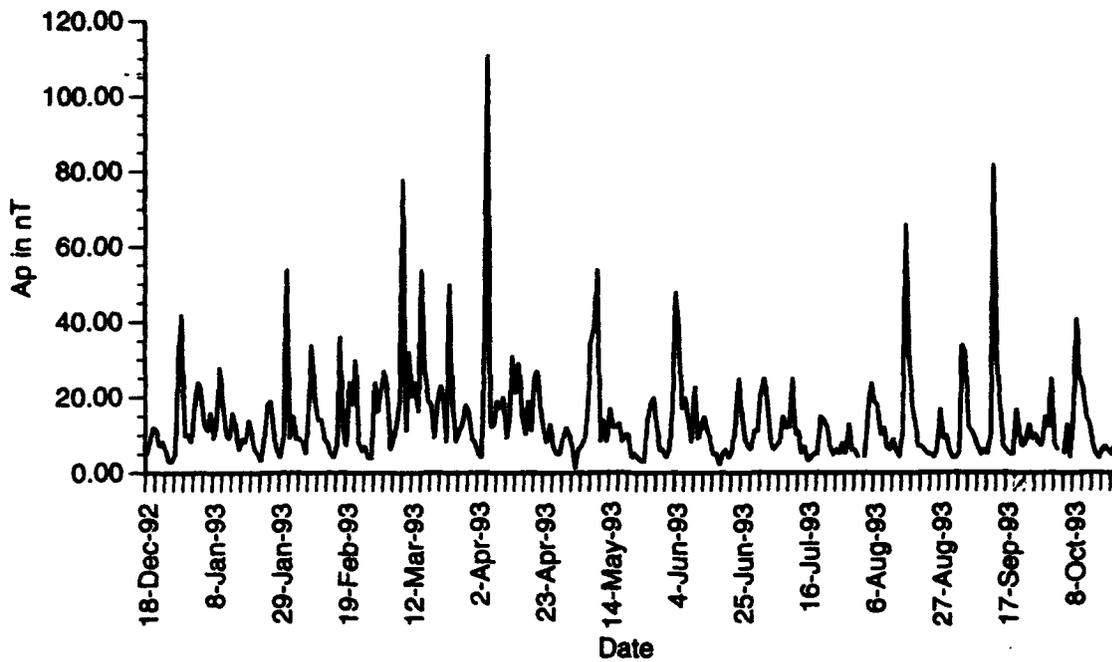
Figure 27: Actual Ap Values

value on left < total F10.7 counts in bin ≤ value on right
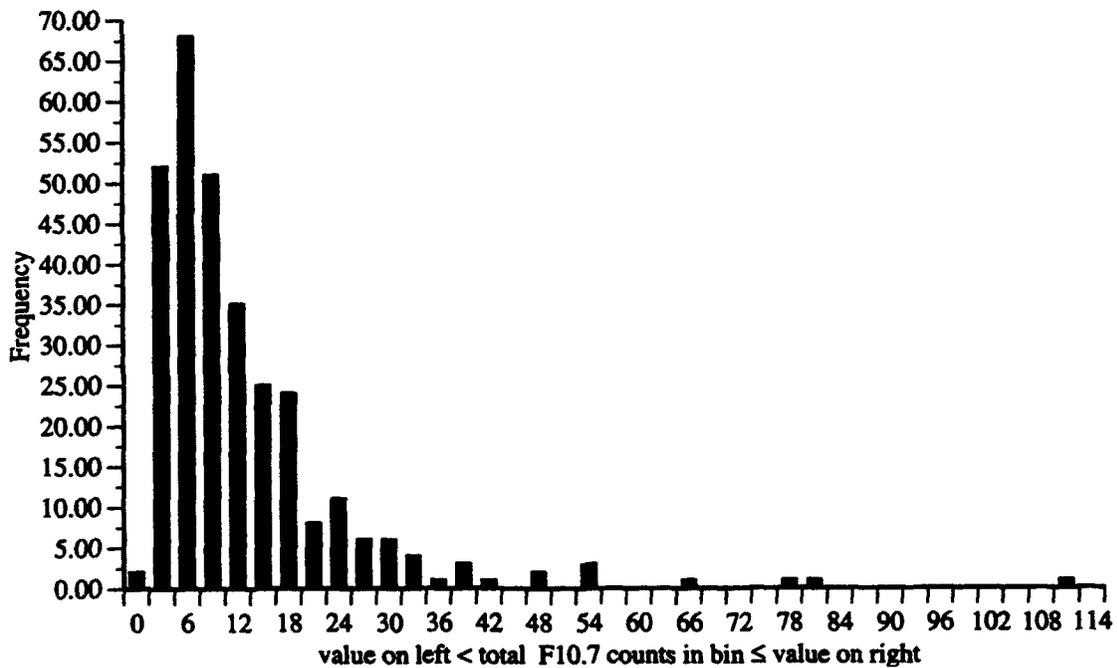
Figure 28: Actual Ap Values' Histogram
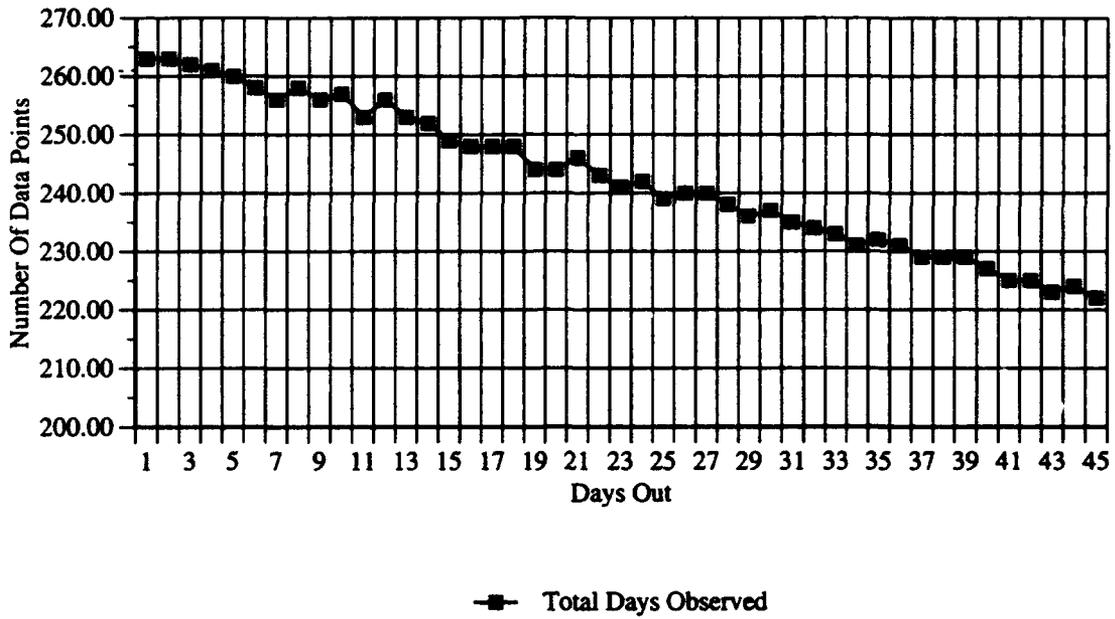
Figure 29: Number of Ap Data Points
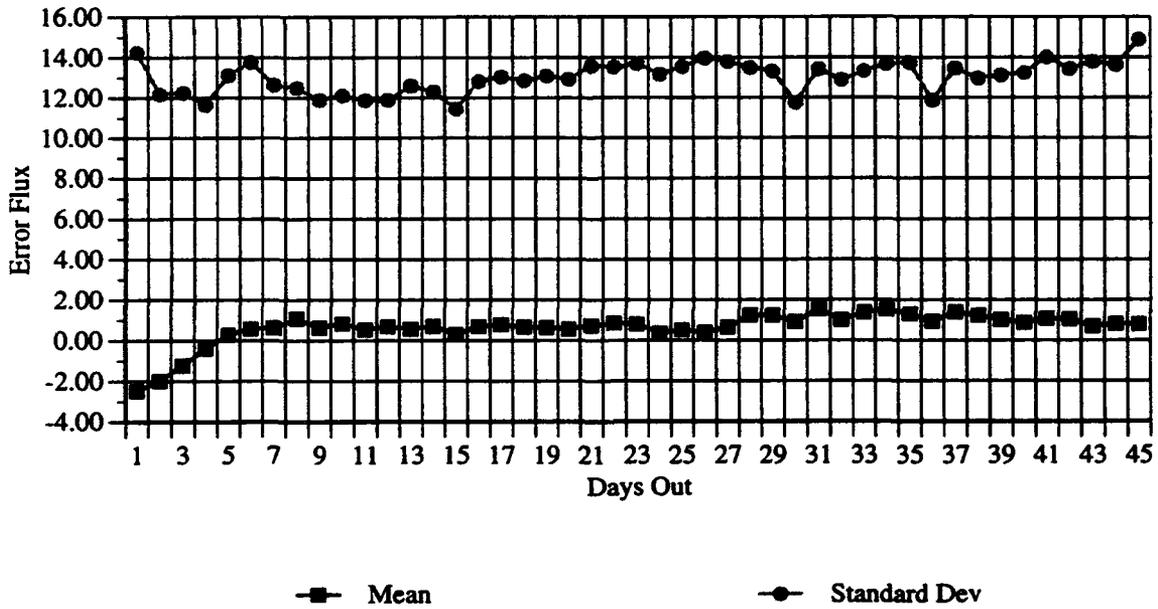
Figure 30: Ap Error Statistics
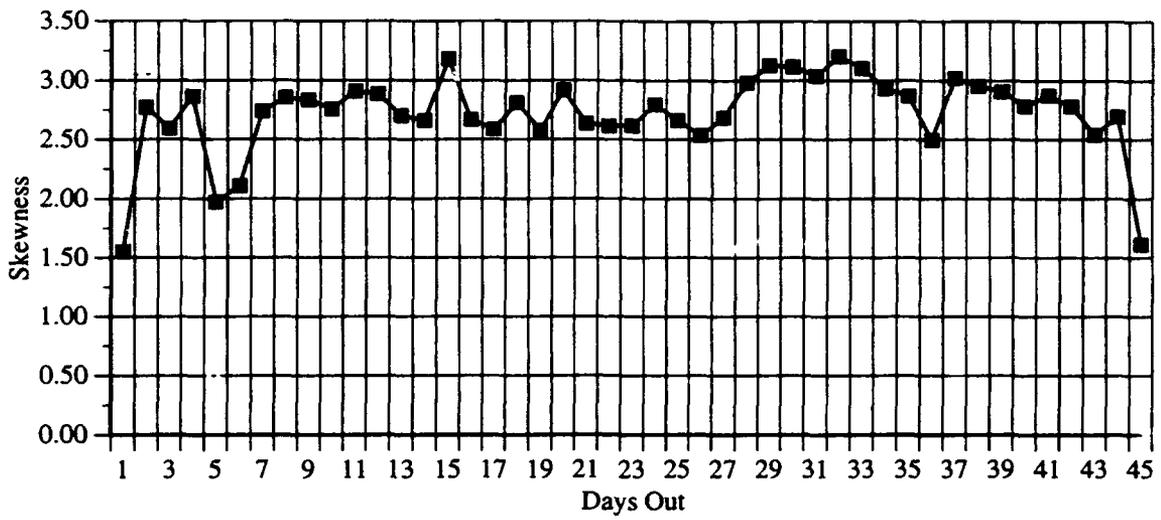
Figure 31: Ap Error Skewness
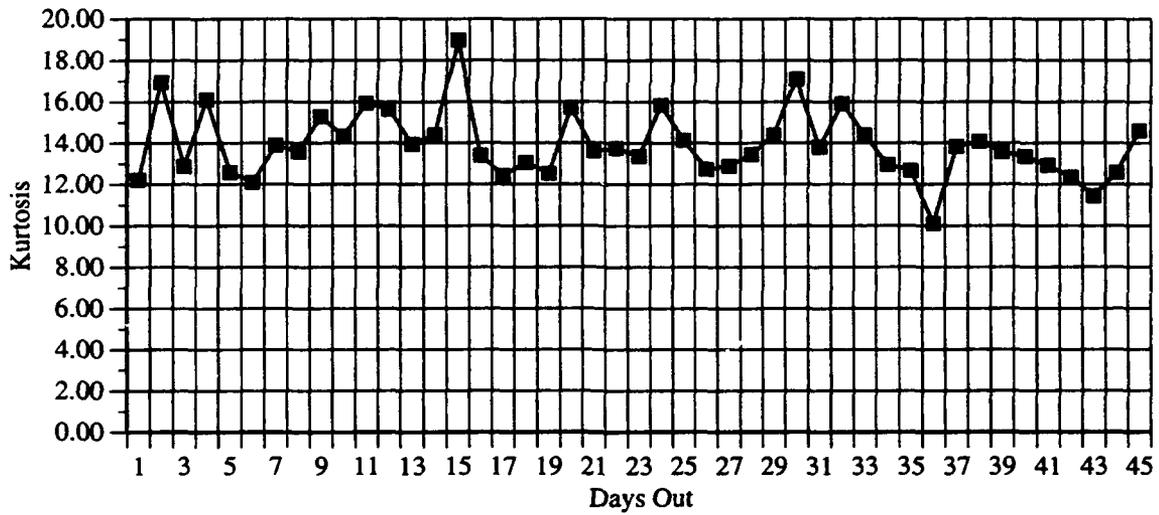
Figure 32: Ap Error Kurtosis

47
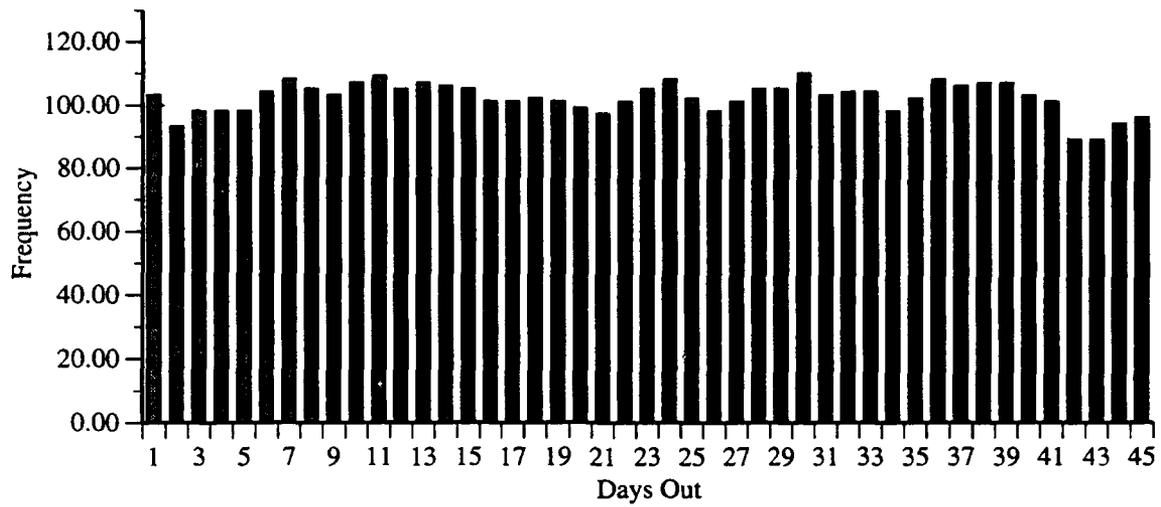
Figure 33: Number of Ap Errors $0 \le x < 5$
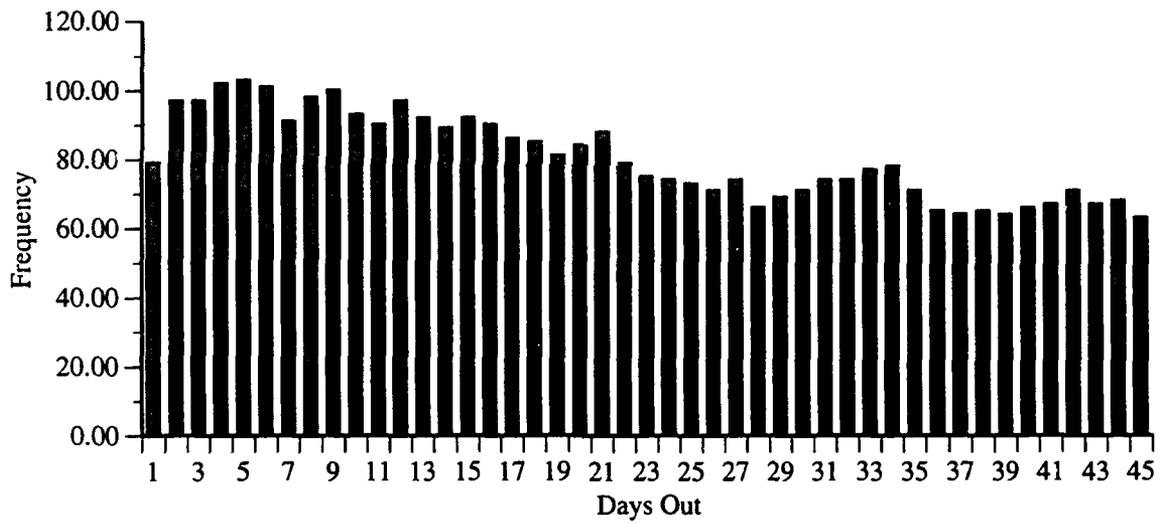
Figure 34: Number of Ap Errors $5 \le x < 10$

48
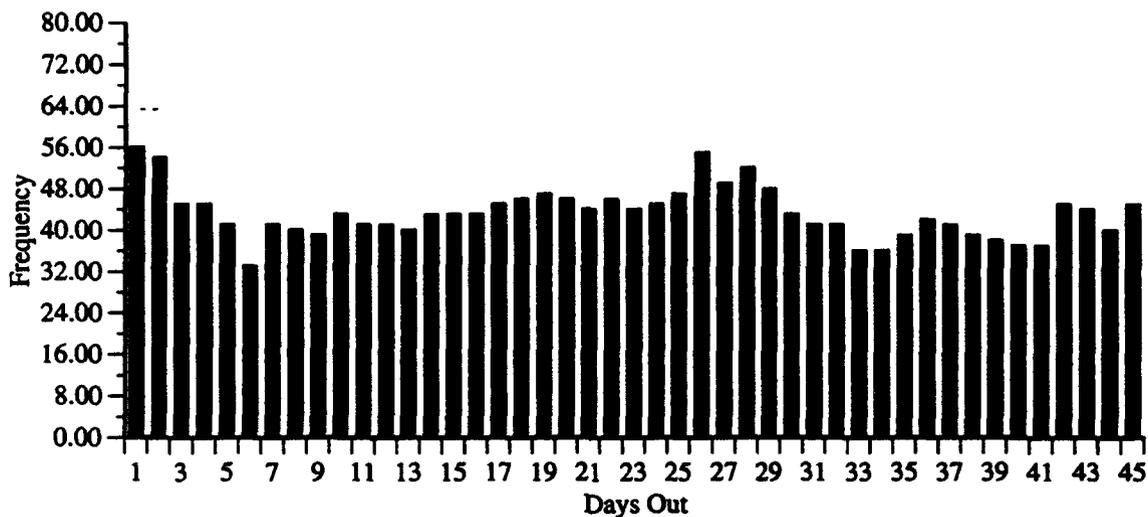
Figure 35: Number of Ap Errors 10 ≤ x < 20
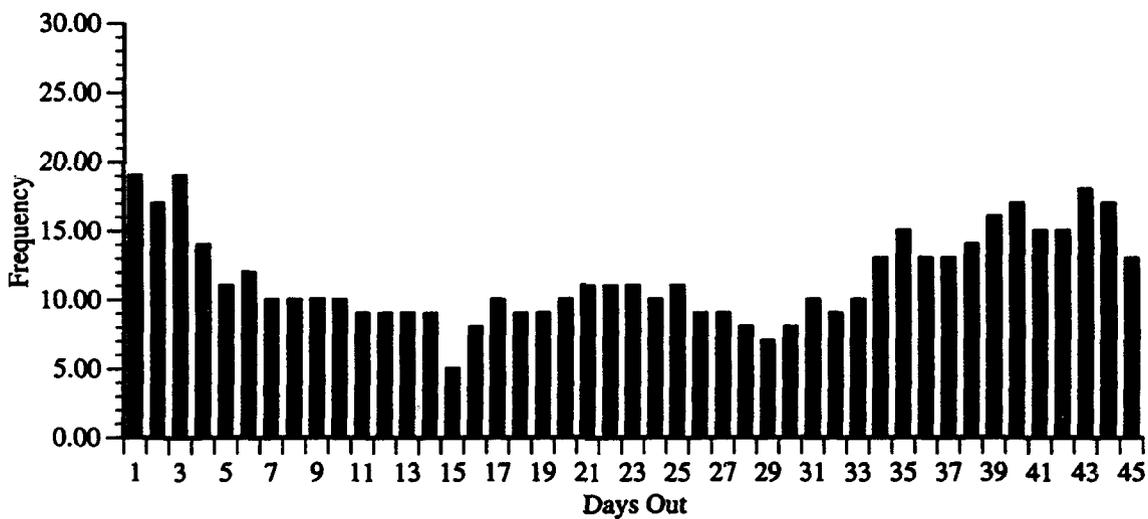
Figure 36: Number of Ap Errors 20 ≤ x < 40
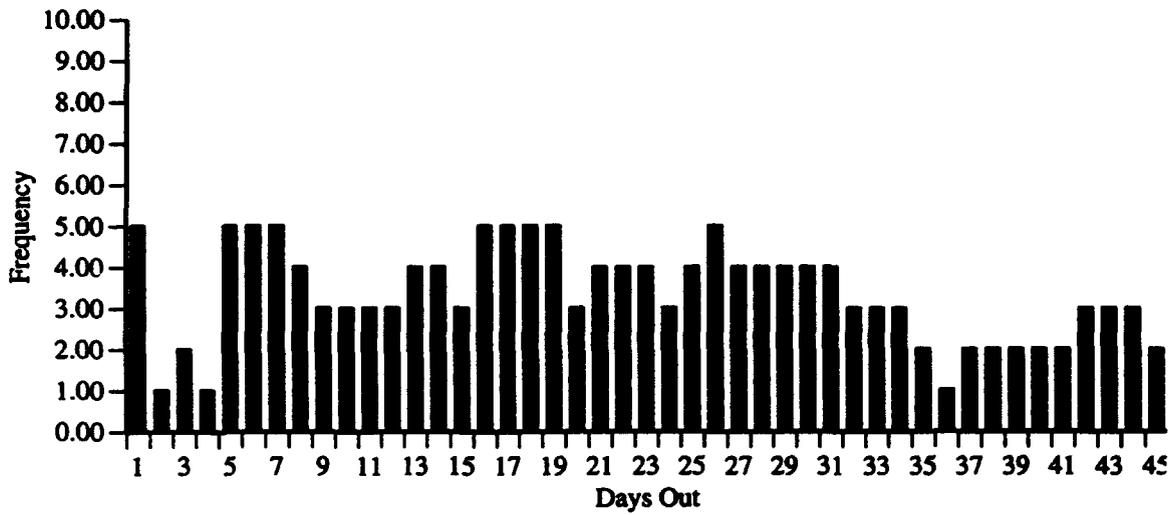
Figure 37: Number of Ap Errors 40 ≤ x < 60
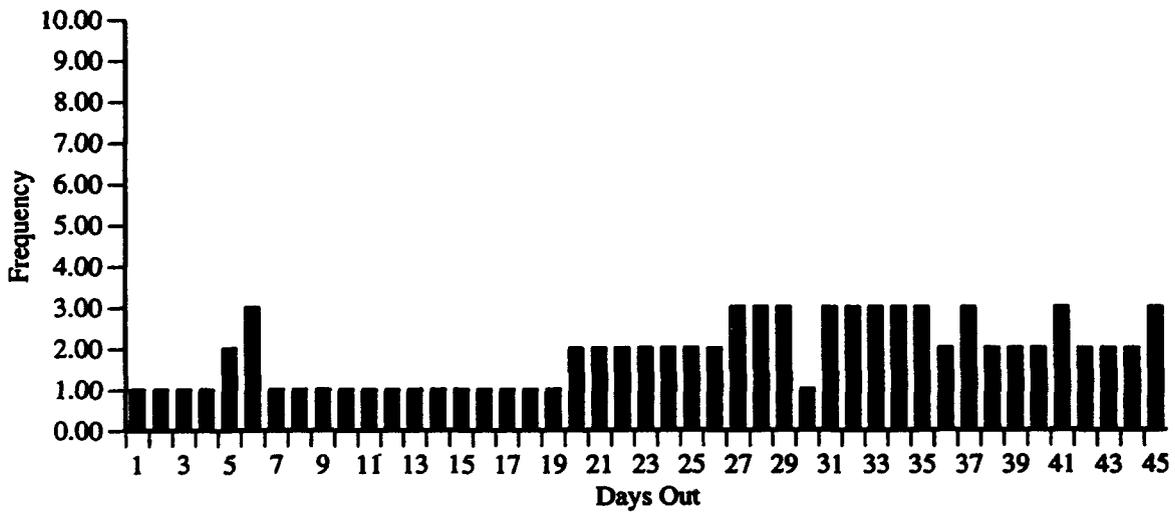
Figure 38: Number of Ap Errors 60 ≤ x

C. LIFETIME 4.1

The errors in forecasted F10.7 and Ap will necessarily produce a different atmospheric density then the actual atmospheric density. If errors of constant magnitude were made daily for 45 days, what effect would this have on orbital lifetimes? Where would the changes be, and what magnitude?

The results of the Lifetime 4.1 F10.7 error modeling are shown in the next sequence of charts. Each chart plots the difference at the end of the 45 day run of either the number of revolutions or the perigee height. Difference is defined as the current parameter minus the reference parameter. Each plot shows the difference as a function of the original starting height of the satellite; where the entering argument (X axis) for each chart is the beginning altitude defined as the semi-major axis minus the radius of the earth. The Y axis gives either the difference in the number of satellite revolutions or the current altitude of perigee. The individual lines are the simulations done at the indicated F10.7 flux level (i.e. 70delta = F10.7 of 70) minus the base flux level (i.e. F10.7=113 for Figures 39 to 48). Therefore each chart will contain a line at 0 difference where the indicated run was charted against the reference level (i.e. F10.7=113 minus F10.7=113). The first 8 charts were generated for various close-to-circular eccentricities (e=.0001, .0004, .0007, & .0010) as an attempt to model realistic satellite orbits. It is seen that an altitude band exists where there are drastic changes in satellite revolution number and in perigee height depending upon the F10.7 value. Additionally, there are altitude bands where large changes in F10.7 will not affect the satellite. Figures 47 and 48 are a 3-D conglomeration of the previous 8 charts as an overview.

Figures 49 to 56 show the differences if the reference level was changed from F10.7=113 to F10.7=70, 156, or 199. These plots were done only for e=.0007. The plotting

51

order is by increasing the F10.7 reference value (70, 113, 156, 199). It is of interest to note that in all the above combinations of F10.7, eccentricity, or beginning altitude, the only appreciable differences are found in a narrow band of altitude, from $250km - 325km$. Here we see drastic differences in both revolution times and perigee altitudes.

It is seen that the errors in forecasting F10.7 over a 45 day period will be a significant effect for satellites operating about the $300km$ altitude range. This is independent of the direction of the error, be it an over-forecasting or under-forecasting of F10.7. It further shows that errors in forecasting F10.7 are not a strong influence in satellites that are below $225km$ or above $350km$. The errors incurred are minimal even with wide fluctuations of F10.7. An example of the magnitude of change from the reference orbit over the 45 day period:

- almost 300 revolutions for a vehicle at $275km$ initial altitude
- over $100km$ difference in perigee height for a vehicle at $300km$ initial altitude

It is now intuitively obvious that a band such as this would occur. Below the band, density is large enough to effectively slow the satellite into a re-entry. Above the band, density is low enough that it is not a major factor in all cases. However, the location and the width of the band were not previously tangible.
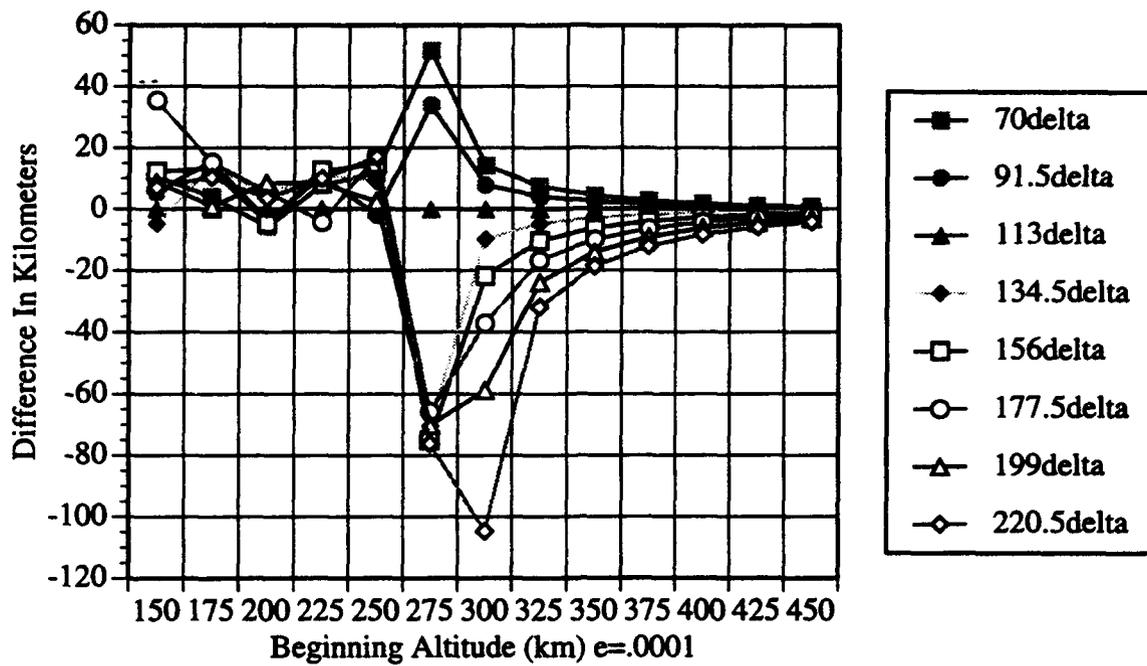
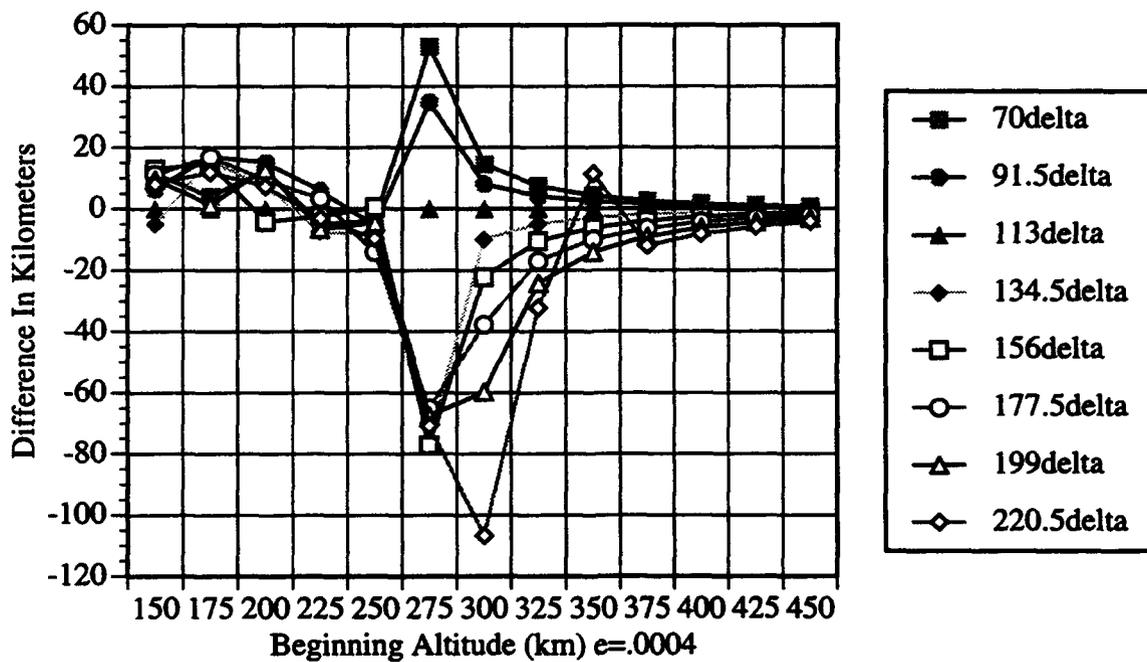**Figure 39: Initial Average Altitude vs. Final Perigee Altitude, F10.7=113**

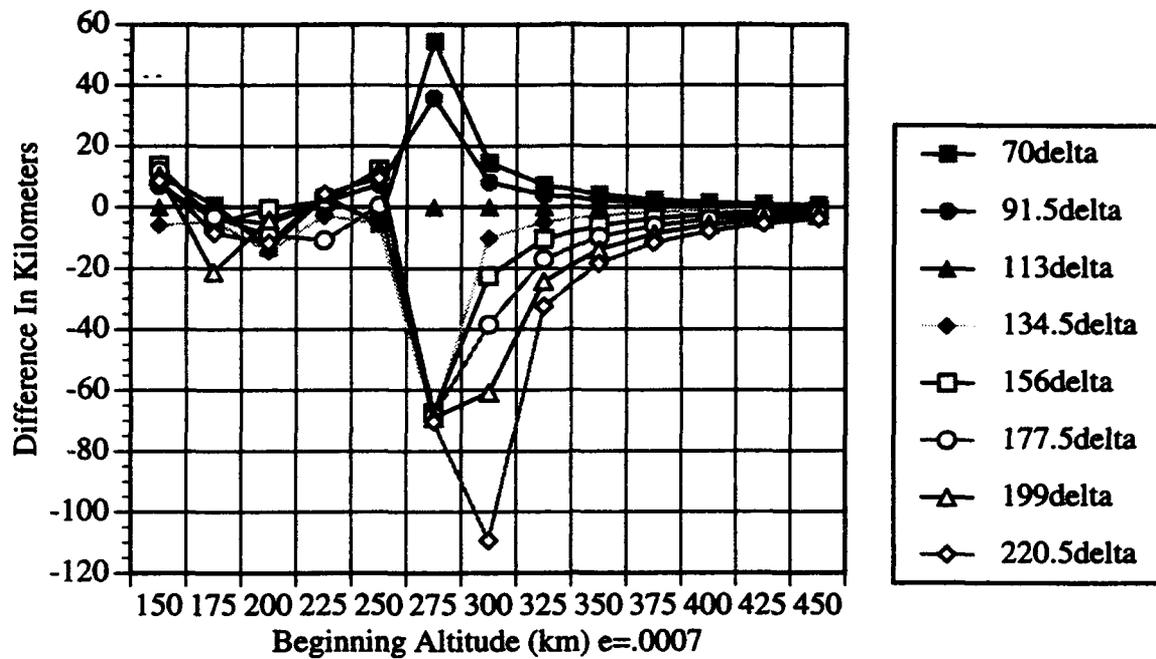**Figure 40: Initial Average Altitude vs. Final Perigee Altitude, F10.7=113**

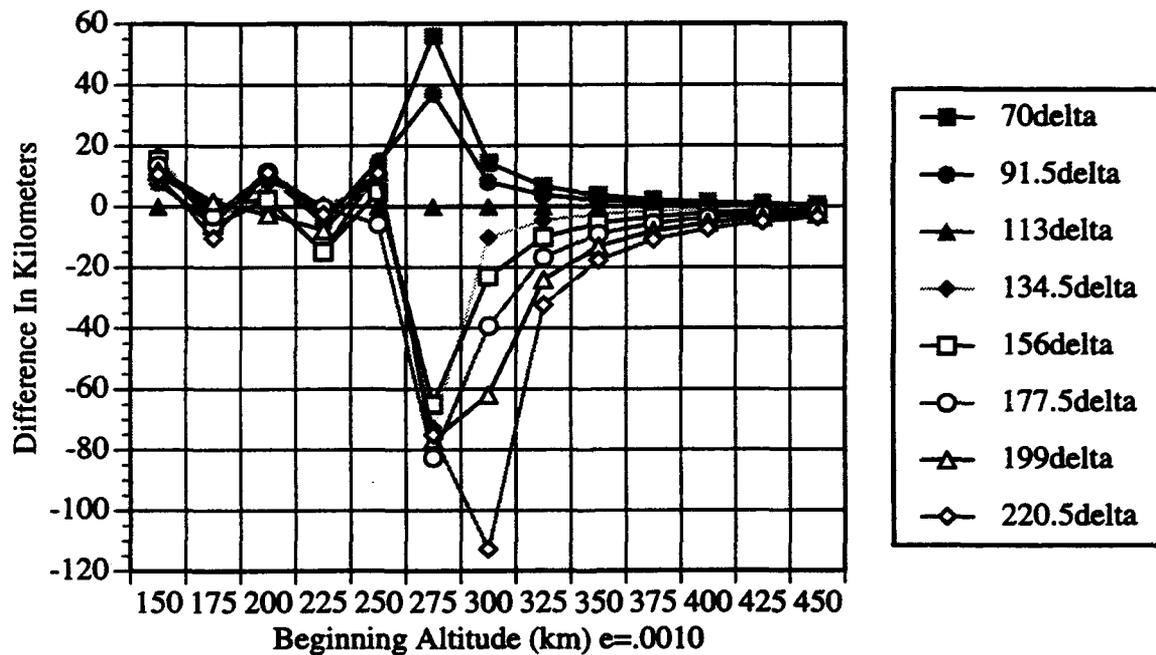**Figure 41: Initial Average Altitude vs. Final Perigee Altitude, F10.7=113**

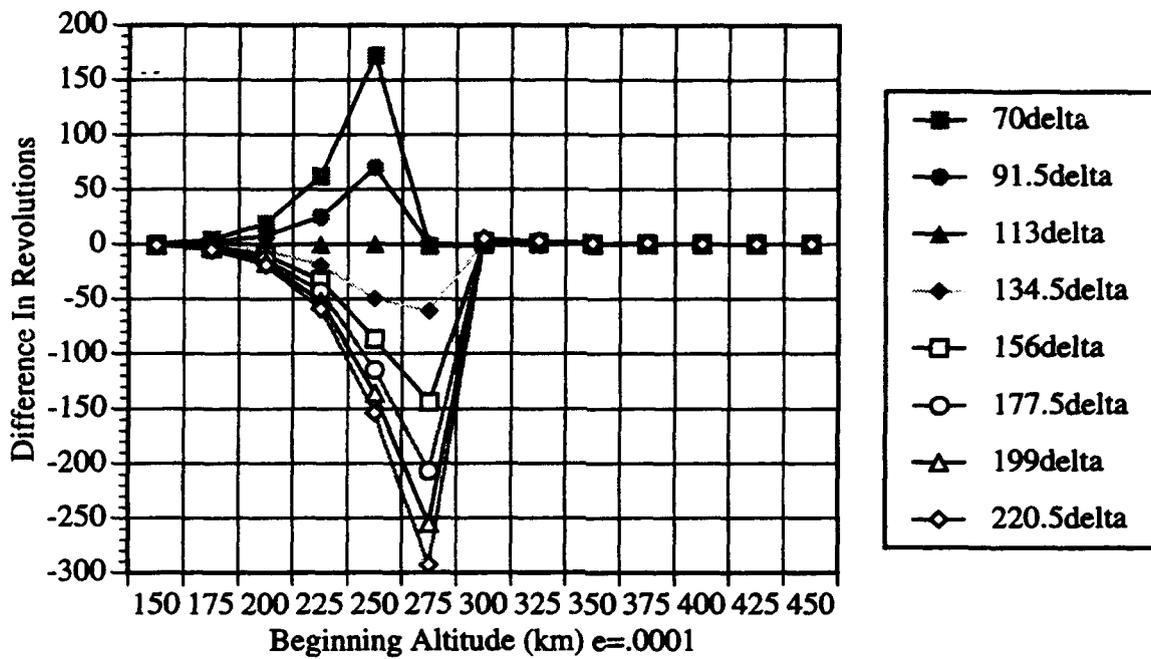**Figure 42: Initial Average Altitude vs. Final Perigee Altitude, F10.7=113**

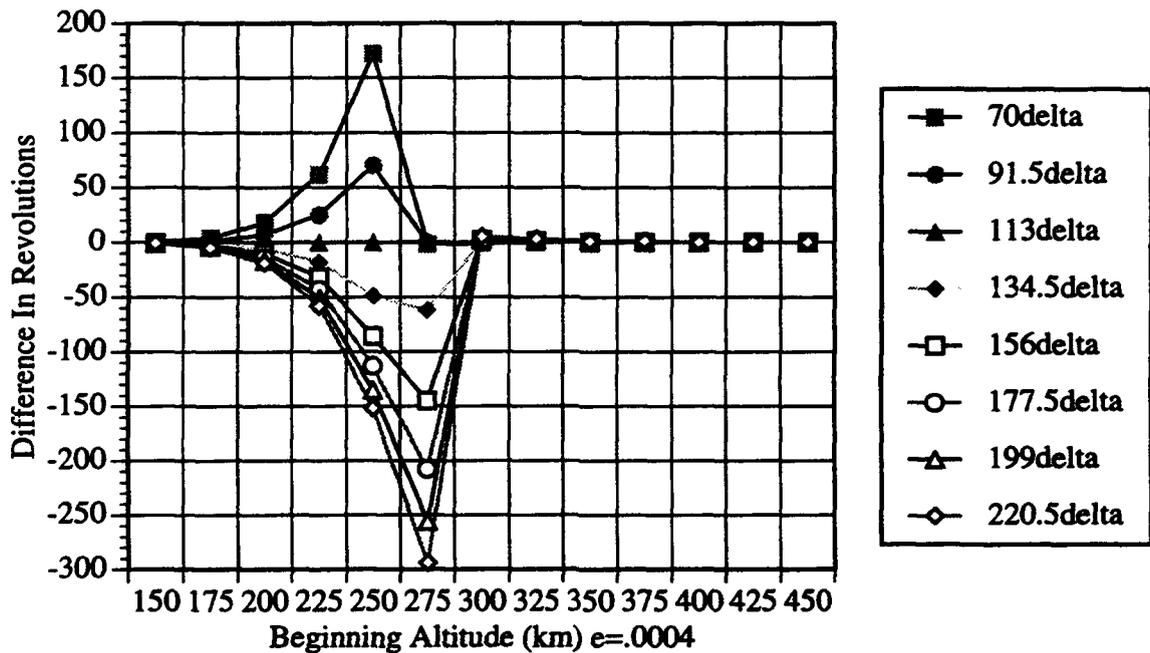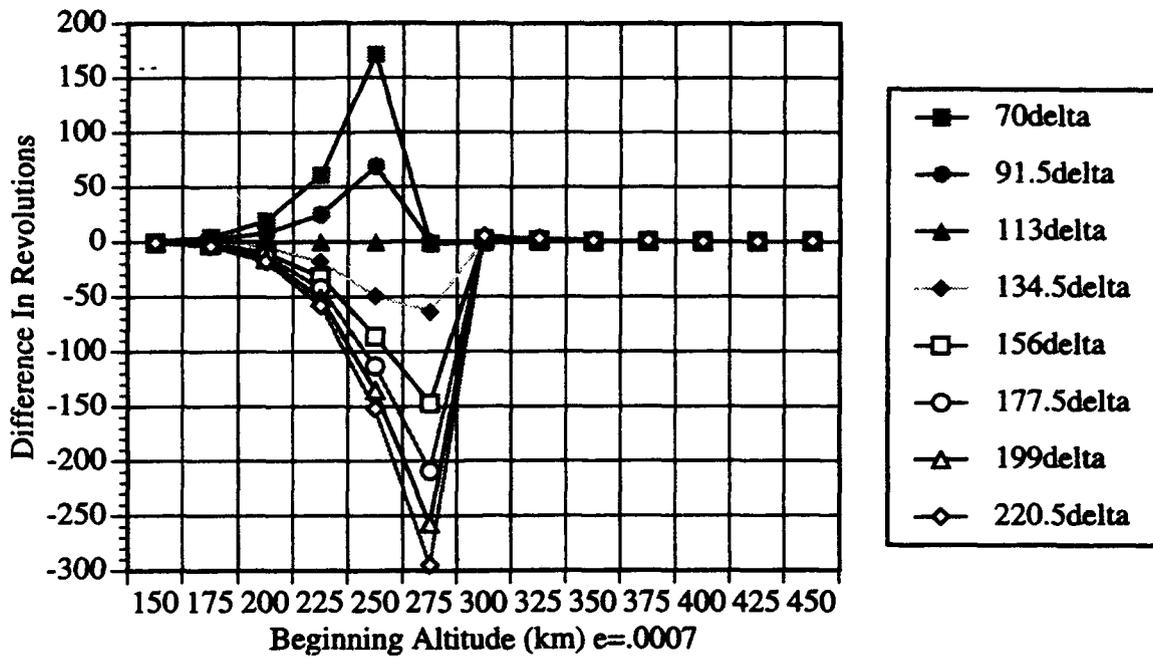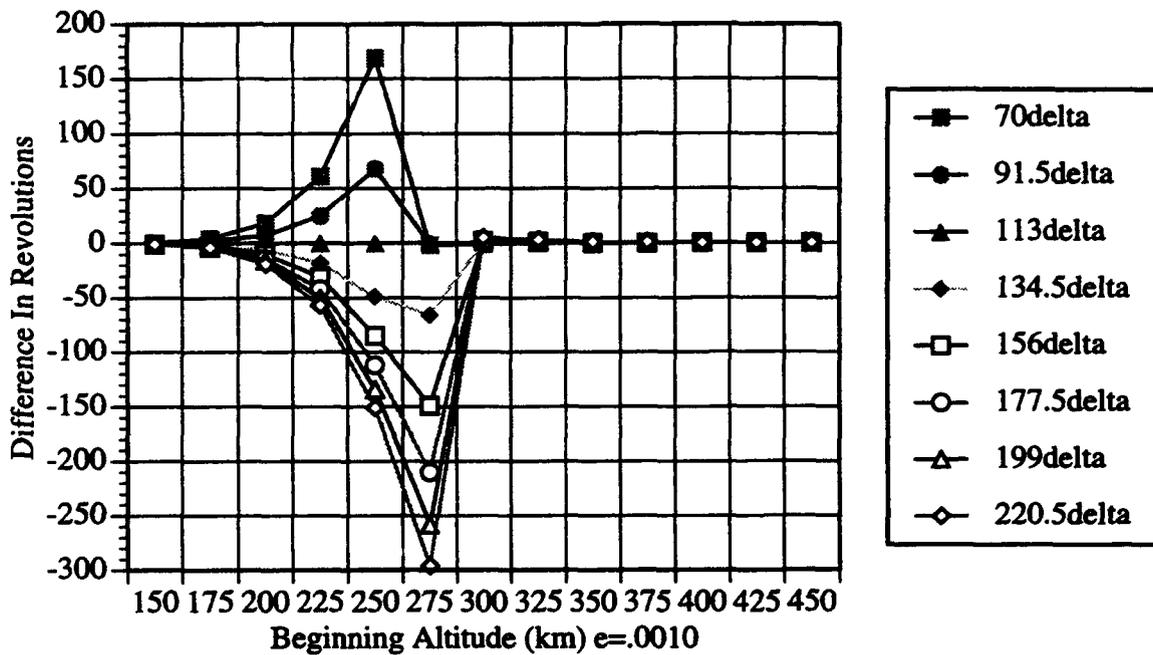**Figure 43: Initial Average Altitude vs. Change In Revolutions, F10.7=113**

Figure 44: Initial Average Altitude vs. Change In Revolutions, F10.7=113

Figure 45: Initial Average Altitude vs. Change In Revolutions, F10.7=113

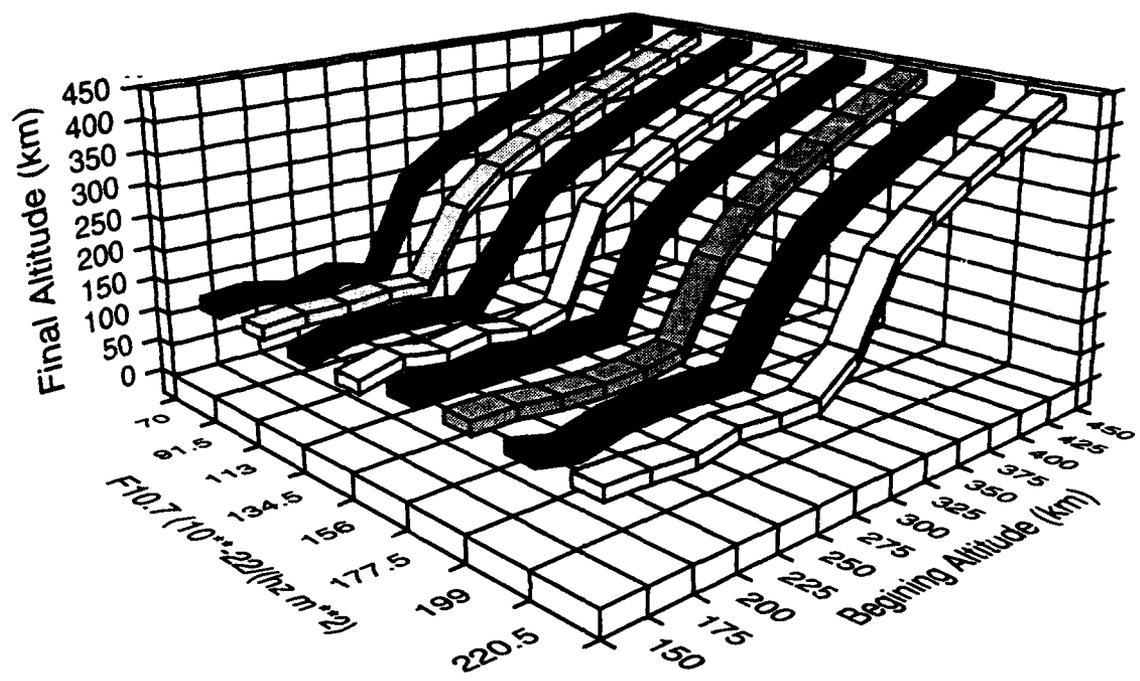**Figure 46: Initial Average Altitude vs. Change In Revolutions, F10.7=113**

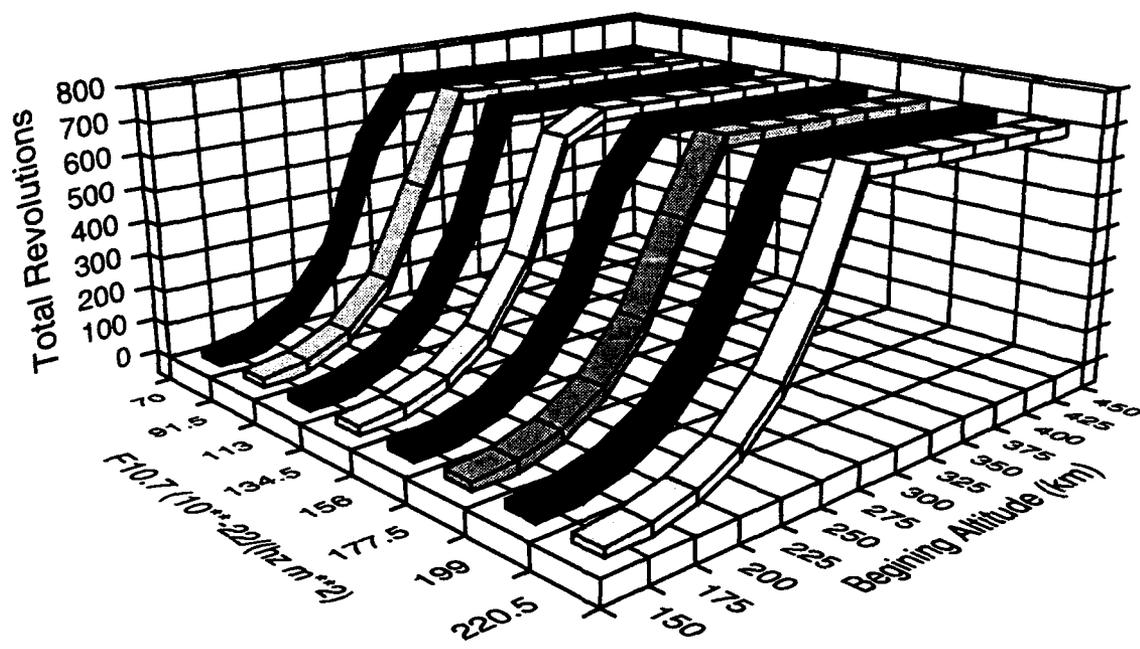**Figure 47: 3-D Overview: Initial Average Altitude vs. Final Perigee Height**

Figure 48: 3-D Overview: Initial Average Altitude vs. Total Revolutions
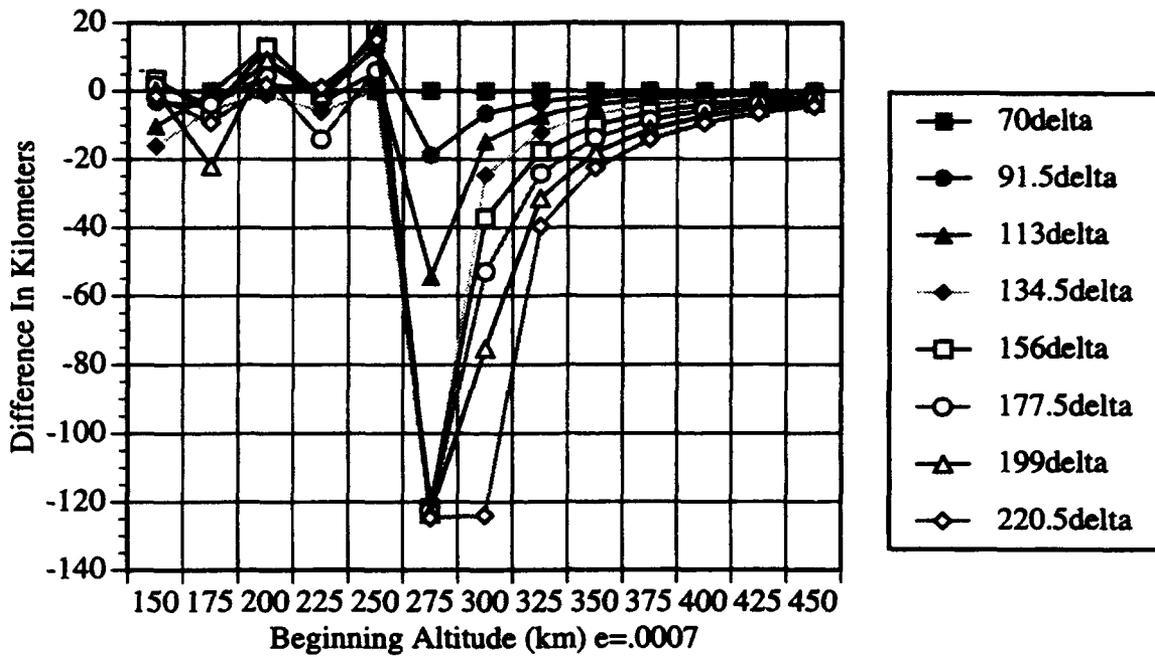
Figure 49: Initial Average Altitude vs. Final Perigee Altitude, F10.7=70
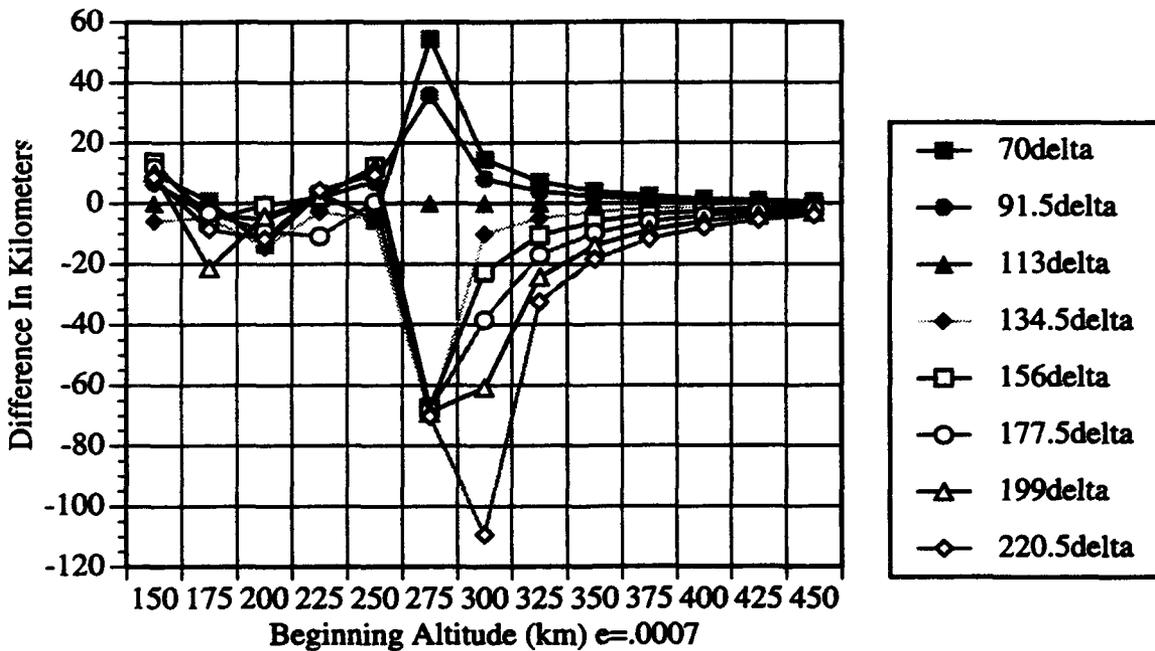

Figure 50: Initial Average Altitude vs. Final Perigee Altitude, F10.7=113
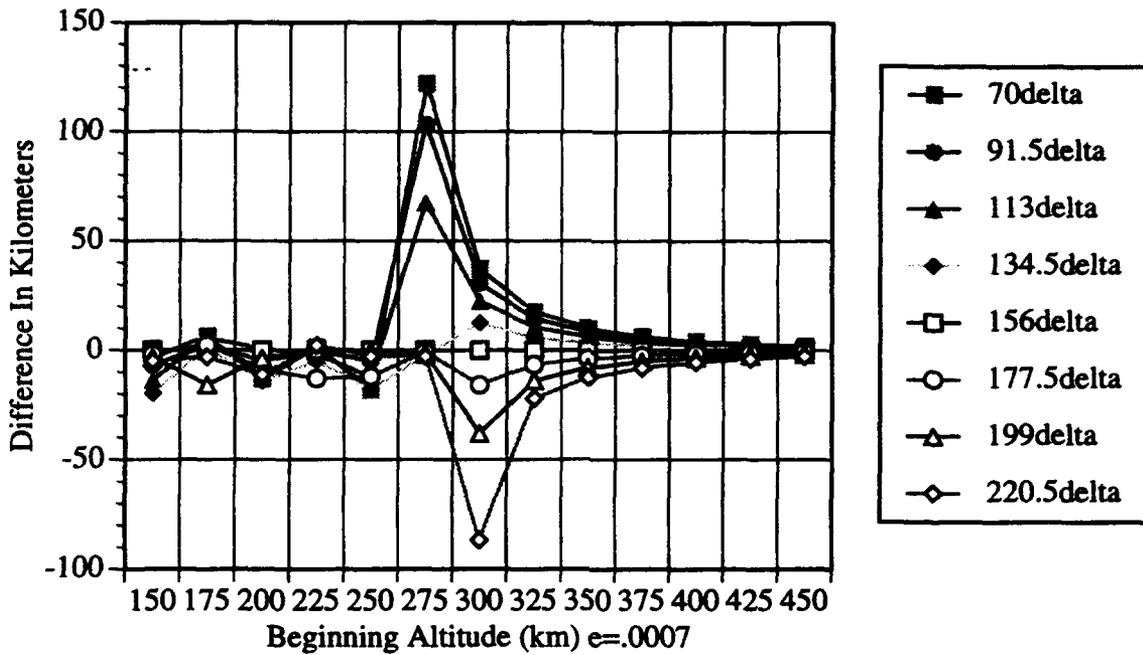
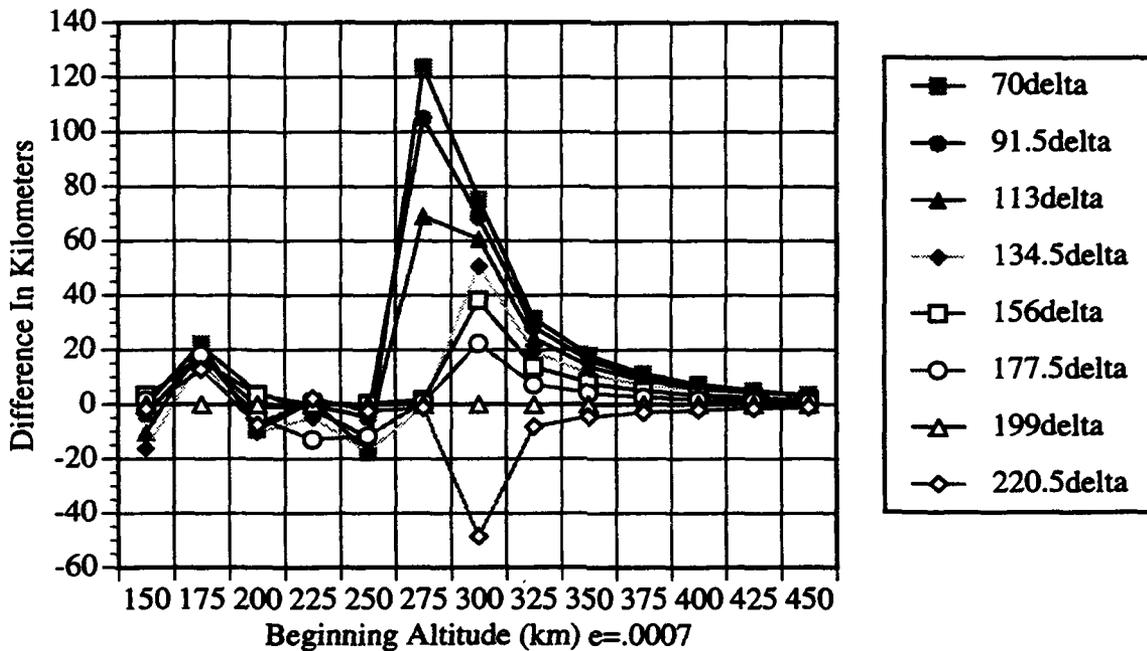**Figure 51: Initial Average Altitude vs. Final Perigee Altitude, F10.7=156**

Figure 52: Initial Average Altitude vs. Final Perigee Altitude, F10.7=199

Figure 53: Initial Average Altitude vs. Change In Revolutions, F10.7=70

Figure 54: Initial Average Altitude vs. Change In Revolutions, F10.7=113

60

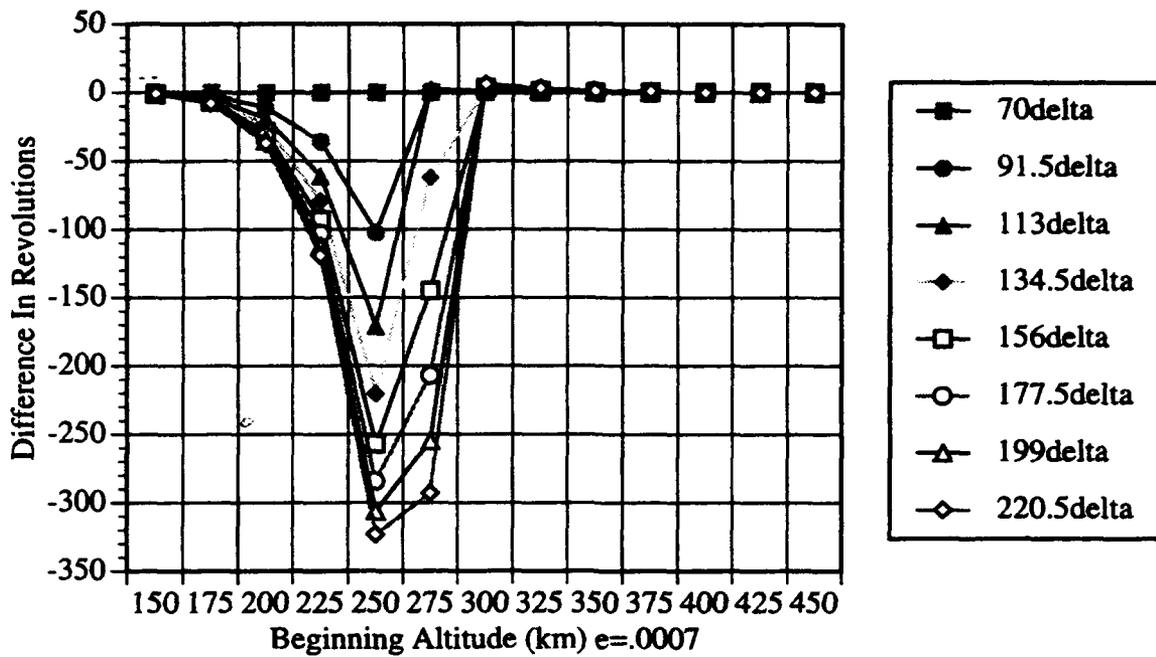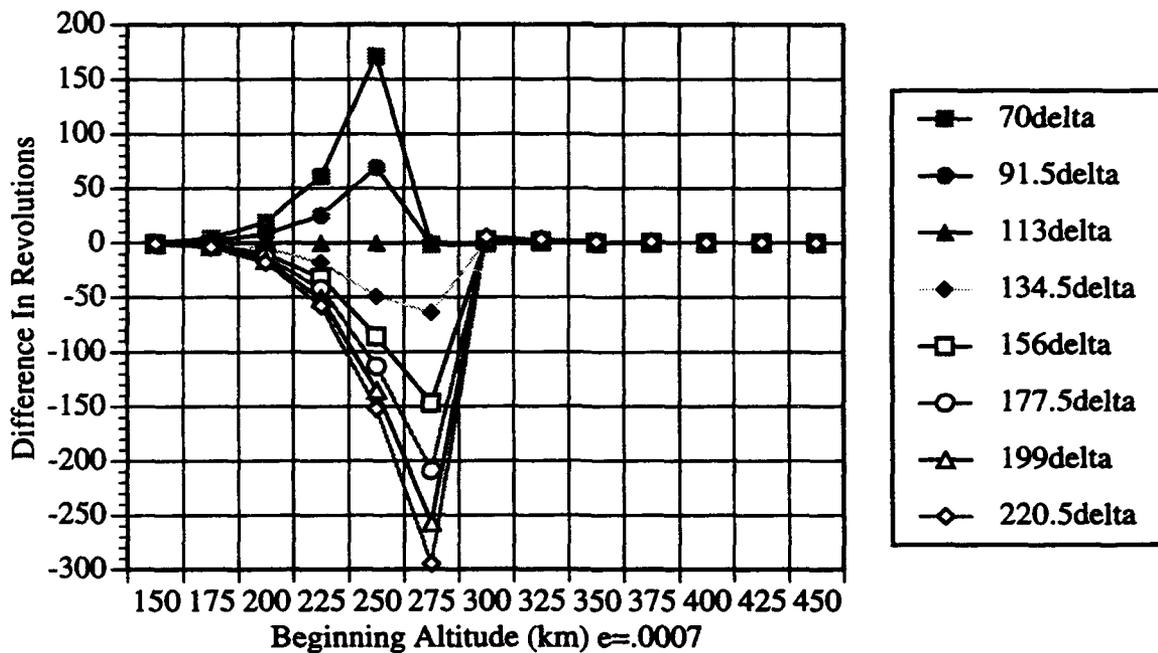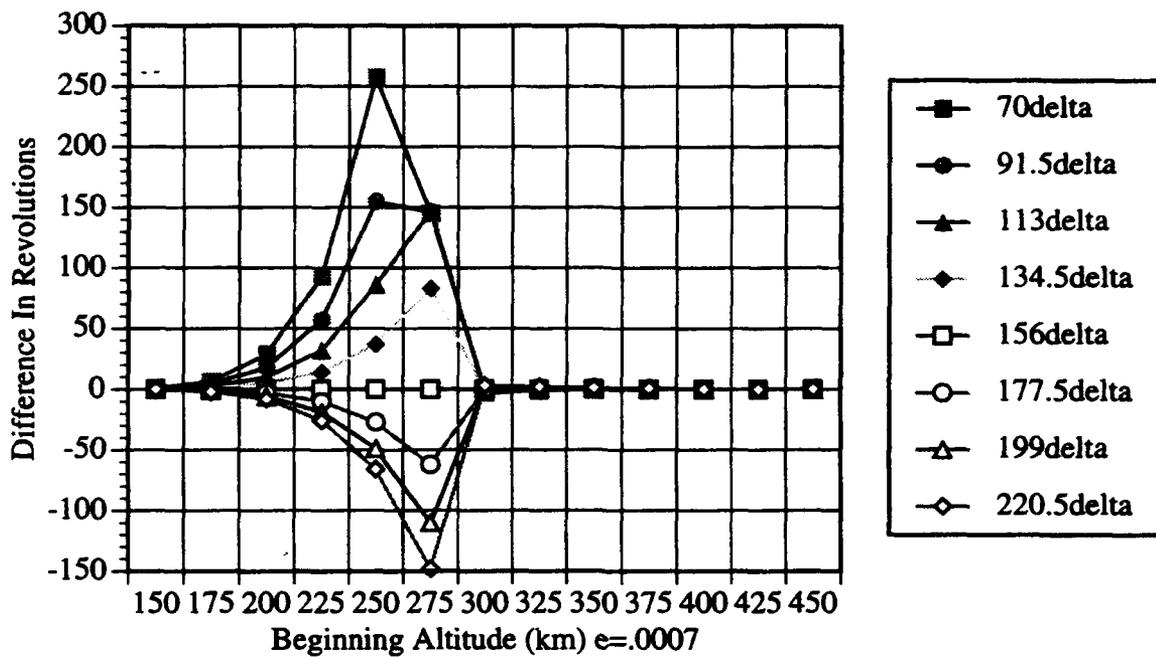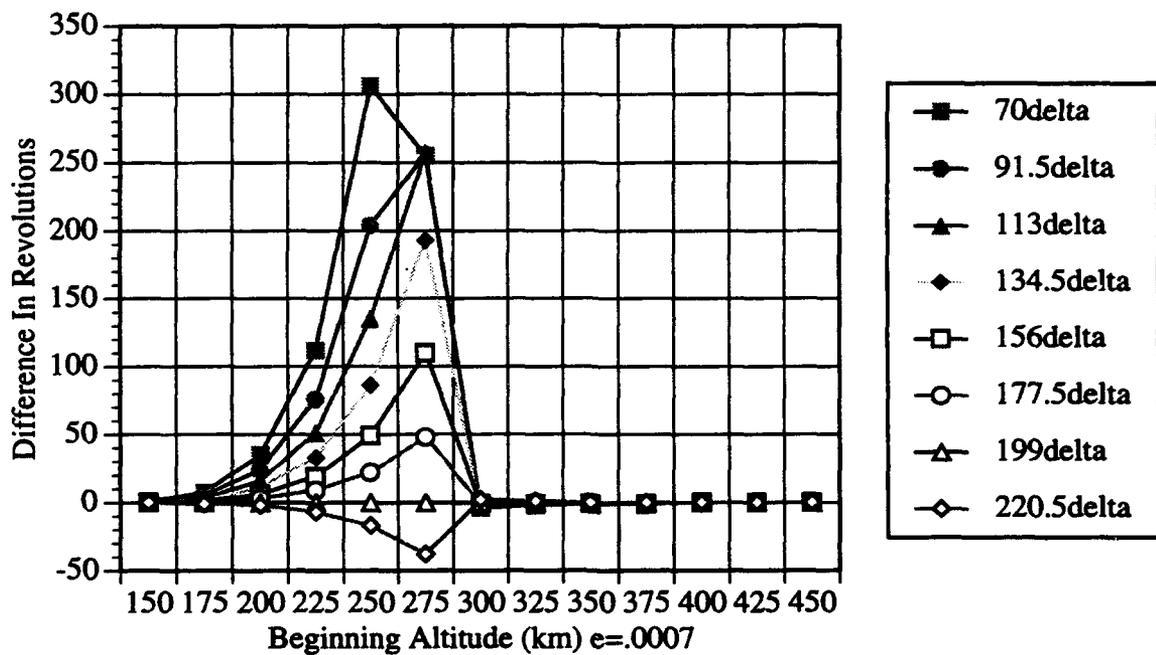**Figure 55: Initial Average Altitude vs. Change In Revolutions, F10.7=156**

Figure 56: Initial Average Altitude vs. Change In Revolutions, F10.7=199

V. CONCLUSIONS AND RECOMMENDATIONS

Forecasting F10.7, and especially Ap, is a challenging task. From the 308 45-day forecasts studied, a few major points are made:

For F10.7:
- Predicted F10.7 values become over-forecasted (i.e. a forecasted value of 150 should be 145) as the predicted day-out gets larger

- From one to seven days-out the forecasted F10.7 values are quite good, with the standard deviation much less than 20 units; beyond the seventh day the standard deviation is fairly constant at 19 units

- There appears to be a trend to over-forecast from 1 day-out to 23 days-out, then under-forecast from 24 to 45 days-out

- The largest errors were made exclusively during the second week-out

For Ap:
- The Ap values showed an approximately 10-day cycle period

- The errors increasingly get worse as time approaches the actual day. From six days-out to one day-out the mean error switches from +1 to -2

- The mean error is very good from six days out to 45 days-out, and is approximately 1

- The standard deviation is large and constant throughout the entire time. Fluctuations are quite high in this variable

- Forecasting for this variable is almost exclusively done by increments of five. Since Ap is a linear representation of a semi-logarithmic variable, more gradations would be appropriate

The effect of changes in F10.7 over a 45 day period appears to affect only a small region of altitudes from about $250km$ to $325km$, regardless of the orbit's initial eccentricity. It thus appears that for re-entry prediction for satellites with altitudes less than $250km$, factors other than F10.7 are more dominate. This, however, needs to be verified by further analysis. The effects of changes in Ap still need to be addressed. Additionally, it is recommended that the actual F10.7 values be used in a vector format to Lifetime 4.1 and compared with the actual data.

LIST OF REFERENCES

[1]   .. Tascione, T. F., *Introduction To The Space Environment*, Orbit Book Company, Inc., 1988

[2]   Jacchia, L. G., "The Earth's Upper Atmosphere -I," *Sky And Telescope*, March, 1975

[3]   Jacchia, L. G., "The Earth's Upper Atmosphere -II," *Sky And Telescope*, April, 1975

[4]   Jacchia, L. G., "The Earth's Upper Atmosphere -III," *Sky And Telescope*, May, 1975

[5]   Larson, W. J., and Wertz, J. R., *Space Mission Analysis and Design*, Microcosm, Inc., 1992

[6]   National Geophysical Data Center / National Oceanic Atmospheric Administration On-Line Bulletin Board System, 1 (303) 497-7319, 8-N-1, Boulder, Colorado

[7]   National Geophysical Data Center / National Oceanic Atmospheric Administration Internet Access: meridian.ngdc.noaa.gov (192.149.148.109), login: online, password: Onl1n3, Boulder, Colorado

[8]   Carovillano, R. L., and Forbes, J. M., *Solar-Terrestrial Physics: Principles and Theoretical Foundations*, D. Reidel Company, 1983

[9]   Heinz, O., "Introduction To The Space Environment," class notes Naval Postgraduate School, Physics 2514

[10]   Akasofu, S., and Chapman, S., *Solar Terrestrial Physics*, Oxford University Press, 1972

[11]   Hess, W. N., *Introduction To Space Science*, Gordon and Breach Science Publishers, 1965

[12]   Halliday, D., and Resnick, J., *Fundamentals of Physics, Third Edition Extended*, John Wiley and Sons, 1988

[13]   Strizzi, J. D., *An Improved Algorithm For Satellite Orbit Decay And Re-Entry Prediction*, Master's Thesis, Massachusetts Institute of Technology, June, 1993

[14]   Flower, P. J., *Understanding The Universe*, West Publishing Company, 1990

[15]   Gedzelman, S. D., *The Science And Wonders Of The Atmosphere*, John Wiley & Sons, 1980

[16]   Chao, C. C., Oltrogge, D., and Strizzi, J. D., *Lifetime 4.1*, Aerospace Corporation, 1993

[17]   Air Force Space Weather Forecast Center, Falcon AFB,

[18]   Jacchia, L. G., *Revised Static Models Of The Thermosphere And Exosphere With Empirical Temperature Profiles*, Smithsonian Astrophysical Observatory Special Report 332, 1971

INITIAL DISTRIBUTION LIST

1. Defense Technical Informational Center   2
   Cameron Station
   Alexandria, VA 22304-6145

2. Library, Code 052   2
   Naval Postgraduate School
   Monterey, CA 93943-5002

3. Dr. I. Michael Ross   4
   Code AA/RO
   Naval Postgraduate School
   Monterey, CA 93943-5002

4. Dr. R. C. Olsen   3
   Code PH
   Naval Postgraduate School
   Monterey, CA 93943-5002

5. Dr. W. B. Colson   1
   Code PH
   Naval Postgraduate School
   Monterey, CA 93943-5002

6. Dr. Joseph Liu   1
   Chief, Astrodynamics Div./CNY
   HQ AFSPACECOM
   150 Vandenberg Street
   Suite 1105
   Peterson, AFB, CO 80194-4025

7. LT John Adler   2
   3284 West Avenida Sombra
   Tucson, AZ 85743